nature portfolio

Peer Review File

ITGB6 modulates resistance to anti-CD276 therapy in head and neck cancer by promoting PF4+ macrophage infiltration

Editorial note: Parts of this Peer Review File have been redacted as indicated to remove third-party material where no permission to publish could be obtained.

REVIEWER COMMENTS

Reviewer #1 (Remarks to the Author): with expertise in head and neck cancer biology and (immuno)therapy

The advent of the current cancer immunotherapy era based on the success of immune checkpoint inhibitors (ICI) has established a shift in the treatment and management of cancer patients. However, most patients do not respond to ICI, primarily targeting PD-1/PD-L1 and CTLA-4 immune checkpoints. This includes head and neck cancer (HNC) patients, with fewer than 20% responding to ICI. Thus, there is an urgency to develop combination therapies to improve response rates and clinical outcomes. Specifically, B7-H3 (CD276) is a member of the B7 family of cell surface proteins that acts as an alternative immune checkpoint. The recent development of enoblituzumab, an investigational anti-B7-H3 humanized monoclonal antibody, has enabled to begin addressing the benefits of targeting CD276 in the clinic. In a recent study (PMCID: PMC9006844), enoblituzumab showed encouraging activity when combined with anti-PD-1. In this single arm combination therapy, 33% of HNC patients showed objective clinical responses, albeit it is unclear the contribution of enoblituzumab to the overall response of the combination treatment, which was not statistically different from historic controls with anti-PD-1 as single agent. In this scenario, Zhang et al have focused in the present study on the mechanisms underlying resistance to α-CD276 therapy, with emphasis in HNC. They took advantage a chemically-induced murine model of HNC, and identified ITGB6 (integrin beta 6 subunit) as a candidate element in treatment response to α-CD276. They propose that: 1) ITGB6 regulates the expression of the tumor-associated chemokine CX3CL1; 2) this chemokine recruits and activates PF4+ macrophages (CX3CR1high); 3) inhibition of the CX3CL1-CX3CR1 axis suppresses PF4+ macrophage recruitment and secretion of CXCL16; 4) and that in turn this reinvigorates cytotoxic CXCR6+CD8+ T cells and 5) enhances the sensitivity to α-CD276 treatment. There are some elements of novelty, but the study seems to address too many aspects and thus the authors reach too many bold conclusions with limited supportive data for each major

finding, which also often over rely on computational analyses that are exploratory in nature rather than by rigorous investigation using orthogonal experimental approaches.

Major concerns:

The study is highly dependent on the use of α-CD276 antibodies. This reviewer could not find a description of the antibody used for anti-tumor studies, only in the context of IHC stainings (line 608) and described as #14058. In this case, this reviewer assumes that it refers to B7-H3 Rabbit mAb #14058, which would not be suitable for the in vivo experiments. In every case, enoblituzumab incorporates an immunoglobulin G1 Fc domain that enhances Fcγ receptor-mediated antibody-dependent cellular cytotoxicity (ADC), thereby engaging the innate immunity. There is no information to suggest that this also the case for the α-CD276 antibody used by the authors, and if so, one can wonder about the overall impact of the findings to guide future clinical evaluation as stated throughout the manuscript.

In this case, it is unclear if the engagement of innate immunity by the α-CD276 antibody (enoblituzumab) will be impacted by the proposed convoluted cell—cell crosstalk initiated by ITGB6 expression in tumor cells on PF4+ macrophages.

While the initial emphasis of the paper is on α-CD276 resistance, the center of the study (and the title) is all about the possibility that ITGB6 modulates resistance to immunotherapy in cancer via PF4+ macrophages. This may imply resistance to ICI, which was not explored?

Regarding the latter, while some evidence suggests activity of enoblituzumab in prostate cancer as single agent, in HNC (the topic of this manuscript) the evidence shows potential increase in the ICI combination setting, which was not explored here.

The authors acknowledge in the discussion that multiple mechanisms may account for ICI (and α-CD276) resistance. However, all their emphasis on ITGB6 appears to be initiated based on scRNAseq from a single mouse resistant to α-CD276 as compared to a single mouse whose tumor size was reduced after α-CD276 treatment, and 2 untreated mice controls (line 131). The reviewer appreciates the elegant bioinformatics analysis of this

experiment, and yet questions the generality of the prediction of ITGB6 as a resistance mechanism base on the limited sampling. This raise concerns over the rest of the studies.

Other concerns:
The tumor response is not clearly defined, as most immunotherapy responses are assessed based on complete responses (clinical or histological) in addition to tumor volume changes.

IHC analysis (e,g., CD8) after 41 days of treatment may reflect more the status of residual disease than relate to the initial antitumoral mechanism (or lack thereof).

In Figure S1C, it is unclear if active caspase staining is in the tumor or stromal cells.

The use of MOC1 cells (including inoculation site) for validation experiments is not clearly justified.

Many of the bold statements throughout the study are correlative in nature, and the biological significance of small changes that are barely statistically significant (eg, Fig 2E, Fig 6H and I, Fig 7A and B, Supp Fig 1B) raise also concerns.

Limited information is provided about PF4+ macrophages and their role in ICI response.

Reviewer #2 (Remarks to the Author): with expertise in cancer immunology, tumor associated macrophages

In this study Caihua Zhang et al, explore the cellular and molecular cues underlying resistance to anti-CD276 based-immunotherapy in murine models of Head and Neck cancer. They find that ITBG6 expressed by tumors is responsible of their resistance to aCD276 treatment. ITGB6 controls CX3CL1 release by the tumor and the attraction of CX3CR1+PF4+ tumor associated macrophages. These macrophages are able to induce CXCR6+CD8+ T cell exhaustion by secreting inhibitory amount of CXCL16. CXCL16 alone is indeed able to promote T cell exhaustion. The study is elegantly conducted and comprise murine genetic models, human relevance and in vitro/in vivo mechanistic experiments. However, additional

experiments should be provided to better understand the role of ITGB6 and CXCL16 in T cell exhaustion.

Some of the main concerns to be addressed in a revised manuscript are listed below.
1- In the induced model: why tumor grow less in KO mice without treatment? Is it T cell mediated? Overall it should be clarified that the reduction in tumor growth after aCD276 treatment of these tumor models (both induced and transplanted) is mediated by CD8 or CD4 T cells. Authors should address this by using anti-CD4 and anti-CD8 depleting Antibodies.

2- Fig3H : scRNAseq
Authors should clarify how they have identified macrophages versus dendritic cells
Usually macrophages express CSF1R and FCGR1 (CD64) while dendritic cells express FLT3.
Some macrophage cluster resemble DCs: for instance CCL17+ Mac could be DCs since DCs are a source of CCL17. Authors should provide the data allowing the reader to identify the clusters.
Another question here: where are type 2 DCs? Type 2 DCs (Mgl2, IRF4) are generally well represented in tumor and often much more abundant than type 1 DCs (Clec9a, IRF8).
Overall, we miss some methodology to fully appreciate the scRNAseq data.

3- Authors show that ITGB6+ tumor recruit PF4+ macrophages through a CX3CL1-CX3CR1 axis. This suggest that PF4+ macrophages are of monocyte origin and locally recruited upon tumor develoment. If true authors should phenocopy their finding by using an anti-CCL2 or anti-CCR2 antibody.

4- Related to my previous comment: In Fig 5I: authors should quantify the other macrophage subsets. Indeed CX3CR1 is expressed by monocytes and blocking this chemokine receptor should reduce all monocyte-derived macrophage subsets in the tumor.

5- Authors switch from their elegant K14-ITGB6fl model to the use of an anti-ITGB6 antibody? This new model of ITGB6 inhibition is not well documented. Can this Ab directly kill tumor cells? Would be important to show a reduction in CX3CL1 and CXCL16 in anti-

ITGB6 treated mice.

6- On the T cell side, authors do not discriminate CD4+ T conventional cells from CD4+ Treg cells. Tregs are key immunosupressive cells in tumors and their functionality is regulated by TGFb, which is itself regulated by ITGB6. Authors should provide data showing no impact of the loss of ITGB6 on Tregs.

7- A novel and surprising finding is the direct role of CXCL16 in the exhaustion of T cells. Is CXCR6 a signaling receptor? To better understand how this chemokine functionnaly impacts T cell differentiation authors should show how CXCL16 impacts T cell states at the transcriptomic level like it has been done for PF4+ macrophages (FigS9)

Minor comments

1- “Before aCD276 treatment, mice are selected in the wt and ko group for similar lesion size.” This should be documented. (line 204)

2- Missing stats in figure 2F (tumor growth curves)

3- In S4C: Clec9+ cells are mark as “Macrophages” in the bar plot but are “DCs” in the UMAP of Fig3H

4- Missing color code in figure 3I for the connecting lines

5- Fig 6D: “Suppressive” is not correct to refer to T cell state. Authors should say “suppressed” or better “terminally exhausted” (=co expressing several inhibitory receptors)

Reviewer #3 (Remarks to the Author): with expertise in (tumor associated) macrophages, transcriptomics

The authors identified ITGB6 expression as essential for resistance of anti-CD276 treatment

in mouse HNSCC. They show that while Itgb6 ablation partially mitigates tumor progression, the combination of Itgb6 knockout and α-CD276 treatment leads to a reduction of tumor size. They also propose that ITGB6 mediates the interaction between tumor cells and PF4+ macrophages by CX3CL1-CX3CR1 axis, with PF4+ macrophages contributing to exhaustion in CXCR6+CD8+ T cells. Finally, they show that signature of PF4+ macrophages is associated with clinicopathological parameters in HNSCC. While the discoveryof ITGB6 expression as essential for resistance of anti-CD276 treatment in mouse HNSCC is interesting, the rest of the data presented are not novel and need to be align with current literature.

No mechanistic data is provided on the role of ITGB6 and why it is essential to resistance of anti-CD276 treatment in mouse HNSCC.

The main issue here is on the nature of PF4+ macrophages. The authors chose to named them based on their expression of PF4. However multiple studies have addressed TAM heterogeneity and this should be added in the context of this study. Especially that the authors have derived a distinct gene signature for these cells using single-cell RNA sequencing, they should look in others studies to what TAM populations they correspond.

Authors should consider compared their data to the recent paper of Pittet laboratory (PMID: 37535729).

The notion that TAM contributed to exhaustion of CD8+ T cells is not novel.

The data showing that signature of PF4+ macrophages is associated with clinicopathological parameters in HNSCC is not convincing. In addition it is well described that TAM are protumoral.

Reviewer #4 (Remarks to the Author): with expertise in CD276 in cancer

This research identifies ITGB6 as a key factor in Enoblituzumab α-CD276 treatment, revealing its role in regulating the expression of CX3CL1 and recruiting PF4+ macrophages, suggesting ITGB6 may be a potential target to overcome resistance in Head and Neck Cancer

therapy. This manuscript has some interesting findings but also has many problems. The research design needs to be more stringent, and several important issues need to be clarified.

Major Concerns:

1. Although the manuscript centers on CD276 therapy, there is not a single figure dedicated to CD276. What is the relationship between CD276 and ITGB6? Does ITGB6 expression correlate with CD276 expression in patient samples? Does ITGB6 regulate Cd276 expression and/or activity?

2. Figure 2F requires clarification on how to explain tumors treated with CTL+CD276 grow faster than CTL+IgG-treated tumors. Ensure statistical analysis is performed on Figure 2 data and clearly stated in the figure.

3. In Figure 2F, comparing cKO+IgG group and cKO+a-CD276 group, although both group showed increased CD8+ cells, only cKO+a-CD276 group showed dramatic increase of Gzmb+Cd8+/Cd8+ ratio. This result indicates that CD8+ cell activation is crucial in anti-CD276 therapy. This observation needs further investigation.

4. The authors need to show if depleting PF4-positive cells will impact the sensitivity of the cells to a-CD276.

5. Does the ITGB6-CX3CL1 axis also recruit other suppressive cells, such as Treg cells, which may also be activated by STAT3?

6. The results of Fig. S2D-F should be shown as the main figures in the article, since these are the key findings of this project.

7. Address issues of poor writing and editing, ensuring proper labeling of figures and supplementary figures for clarity. The figure # and supplementary figure# are not labeled which makes the manuscript very difficult to read.

Minor concerns,

1. The abstract: “Enoblituzumab is an immunotherapeutic agent targeted at CD276, demonstrating both safety and efficacy in the activation of T cells and oligodendrocyte-like cells against a variety of cancers. Nonetheless, numerous patients have not realized clinical benefits, and the mechanisms underlying resistance to α-CD276 therapy remain inadequately understood.” Enoblituzumab has not been approved by the FDA for patient treatment yet. Thus, this statement is not applicable.

2. The introduction should be more comprehensive and reader friendly, providing context on the significance of PF4+ Macrophages and GZMB+ T cells.

3. Fig. 1, the labels in Fig. 1F and 1K, “stress” or “sress”?

4. Fig. 2C: The ITGB6 KO tongue tissue seems to bear more tumor. How do you quantify the tumor size and mass?

5. Fig. 4E: The text mentions that ITGB6 KO downregulates CX3CL1 mRNA transcription, by what experiment?

6. Fig. S4F: The text mentions that this figure shows a CX3CL1 decrease when knockout ITGB6 in IHC, but the data is somehow vague, do you have a western blotting result?

7. Fig. S4I: Lack of labeling, STAT3 IP/ IgG IP?

8. The title needs to be more specific to CD276 targeting immunotherapy.

We sincerely appreciate the invaluable comments and insights provided by the reviewers. We have thoroughly considered their critiques and suggestions, and have made diligent efforts to address all concerns raised. Significant new data have been added to both the main and supplementary figures, directly responding to the issues highlighted in the initial review. As a result, our manuscript has been substantially improved, offering a stronger and clearer presentation of our findings. We are grateful for the reviewers' guidance, which has considerably enhanced our research. Furthermore, we thank the reviewers for their patience during the extended revision process, necessitated by the comprehensive experimental work required. Their understanding and willingness to evaluate the revised manuscript are highly appreciated.

Reviewer #1

The advent of the current cancer immunotherapy era based on the success of immune checkpoint inhibitors (ICI) has established a shift in the treatment and management of cancer patients. However, most patients do not respond to ICI, primarily targeting PD-1/PD-L1 and CTLA-4 immune checkpoints. This includes head and neck cancer (HNC) patients, with fewer than 20% responding to ICI. Thus, there is an urgency to develop combination therapies to improve response rates and clinical outcomes. Specifically, B7-H3 (CD276) is a member of the B7 family of cell surface proteins that acts as an alternative immune checkpoint. The recent development of enoblituzumab, an investigational anti-B7-H3 humanized monoclonal antibody, has enabled to begin addressing the benefits of targeting CD276 in the clinic. In a recent study (PMCID: PMC9006844), enoblituzumab showed encouraging activity when combined with anti-PD-1. In this single arm combination therapy, 33% of HNC patients showed objective clinical responses, albeit it is unclear the contribution of enoblituzumab to the overall response of the combination treatment, which was not statistically different from historic controls with anti-PD-1 as single agent. In this scenario, Zhang et al have focused in the present study on the mechanisms underlying resistance to α-CD276 therapy, with emphasis in HNC. They took advantage a chemically-induced murine model of HNC, and identified ITGB6 (integrin beta 6 subunit) as a candidate element in treatment response to α-CD276. They propose that: 1) ITGB6 regulates the expression of the tumor-associated chemokine CX3CL1; 2) this chemokine recruits and activates $PF4^+$ macrophages (CX3CR1high); 3) inhibition of the CX3CL1-CX3CR1 axis suppresses $PF4^+$ macrophage recruitment and secretion of CXCL16; 4) and that in turn this reinvigorates cytotoxic $CXCR6^+CD8^+$ T cells and 5) enhances the sensitivity to α-CD276 treatment. There are some elements of novelty, but the study seems to address too many aspects and thus the authors reach too many bold conclusions with limited supportive data for each major finding, which also often over rely on computational analyses that are exploratory in nature rather than by rigorous investigation using orthogonal experimental approaches.

Response: Thank you so much for your comments and suggestions. We have revised our manuscript according to your suggestions. Below are the point-to-point responses

and new data to address your helpful comments:

1. The study is highly dependent on the use of α-CD276 antibodies. This reviewer could not find a description of the antibody used for anti-tumor studies, only in the context of IHC stainings (line 608) and described as #14058. In this case, this reviewer assumes that it refers to B7-H3 Rabbit mAb #14058, which would not be suitable for the in vivo experiments. In every case, enoblituzumab incorporates an immunoglobulin G1 Fc domain that enhances Fcγ receptor-mediated antibody-dependent cellular cytotoxicity (ADC), thereby engaging the innate immunity. There is no information to suggest that this also the case for the α-CD276 antibody used by the authors, and if so, one can wonder about the overall impact of the findings to guide future clinical evaluation as stated throughout the manuscript. In this case, it is unclear if the engagement of innate immunity by the α-CD276 antibody (enoblituzumab) will be impacted by the proposed convoluted cell—cell crosstalk initiated by ITGB6 expression in tumor cells on $PF4^+$ macrophages.

Response: We express our gratitude to the reviewer for their insightful comments. Since enoblituzumab was mentioned at the outset of the abstract, and our subsequent experiments utilized this treatment without explicit clarification, leading to potential ambiguity, we have now included the specific product code information for the enoblituzumab antibody (MCE, cat#HY-P9966). In the revised manuscript, detailed explanations have been added concerning the in vivo therapeutic antibodies utilized in our study. Below, we have listed the specific updates made in the revised version.
Methods: In our CD276 blockade therapy experiments, we treated mice through a regimen of intraperitoneal injections. More precisely, mice received either the carrier IgG control (InVivoMAb rat IgG1 isotype control, BioXcell, Catalog #BE0088, at a dosage of 10 mg/kg body weight) or the anti-CD276 antibody (enoblituzumab, MCE, Catalog #HY-P9966, also at 10 mg/kg body weight), following a four-day cycle for six weeks. For the specific depletion of $CD8^+$ T lymphocytes, we performed intraperitoneal injections of anti-CD8 (InVivoPlus anti-mouse CD8α, BioXcell, Catalog #BP0061, at 100 μg per mouse) . Similarly, $CD4^+$ T cells were depleted using anti-CD4 (InVivoPlus anti-mouse CD4, BioXcell, Catalog #BE0119, at 100 μg per mouse) every 4 days, extending over six weeks in the induced model and 20 days in the transplanted model.

2. While the initial emphasis of the paper is on α-CD276 resistance, the center of the study (and the title) is all about the possibility that ITGB6 modulates resistance to immunotherapy in cancer via $PF4^+$ macrophages. This may imply resistance to ICI, which was not explored? Regarding the latter, while some evidence suggests activity of enoblituzumab in prostate cancer as single agent, in HNC (the topic of this manuscript) the evidence shows potential increase in the ICI combination setting, which was not explored here.

Response: We are grateful for the reviewer's constructive suggestions. In response, we established a mouse cohort resistant to PD1 therapy, adhering to the methodology you recommended. To explore the role of ITGB6 in mediating resistance to α-PD1 therapy, we employed a comparable approach and administered α-PD1 or IgG to 4NQO-induced carcinogenic mice for 13 days. The α-PD1 was delivered intraperitoneally at a dose of 10 mg/kg every four days, consistent with previous protocols, amounting to four total doses (Fig. 9A). Tumor progression was monitored bi-weekly from the initial α-PD1 administration via MRI (Fig. 9B). Resistance was characterized by an early response in MRI imaging followed by an increase to more than 120% of the initial size, according to RECIST criteria (Fig. 9B). Thirteen days after the first injection, tongues of the HNSCC-bearing mice were removed (Fig. 9C), revealing reduced malignancy, invasion area, and tumor count in the αPD1-sensitive group compared to the control and resistant groups (Fig. 9C). IHC analysis showed a marked decrease in ITGB6 expression in the sensitive group (Fig. 9D). Furthermore, increased infiltration of $PF4^{+}$ macrophages was observed in the resistant group (Fig. 9E). To determine ITGB6's contribution to α-PD1 treatment efficacy, 12 αPD1-resistant mice were divided into two groups: one continued with the PD1 antibody while the other was treated with a combination of PD1 and the ITGB6 antibody 264RAD. This method notably restored α-PD1 treatment responsiveness in the mice (Fig. 9F and G). The overall analysis of lesion quantity and area demonstrated that ITGB6 inhibition reinstates α-PD-1 treatment sensitivity in mice (Fig. 9H and I). Below, we provide detailed descriptions and images incorporated into the manuscript to highlight these results (New Figure 9). As indicated in our a-PD1 treatment data, ITGB6 appears to be a common mechanism in resistance to immune checkpoint inhibitor. Hence, blocking ITGB6 would likely be beneficial in either single agent or combination therapy scenario.

[figure redacted]

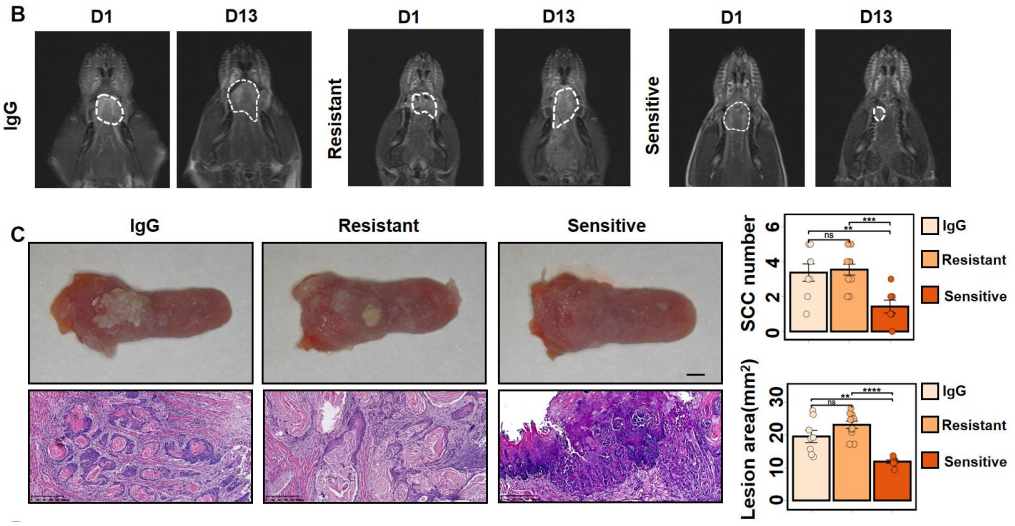

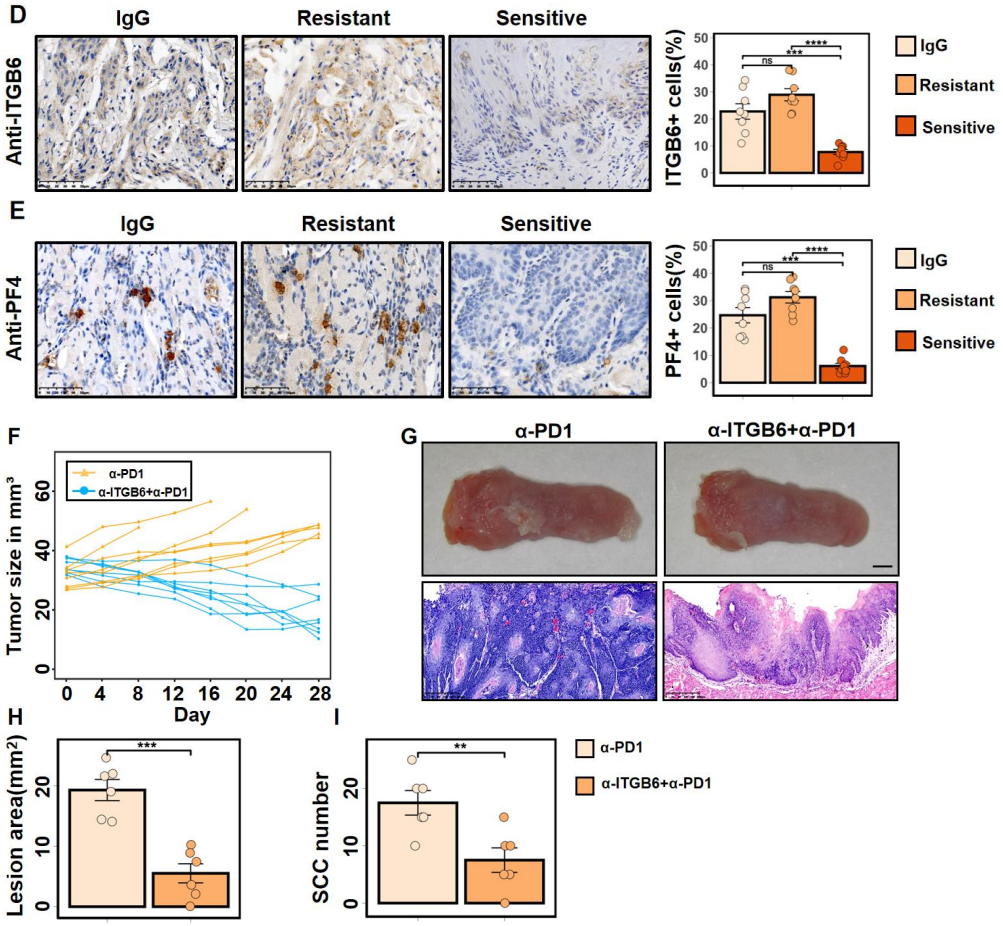

New Figure 9. A.The experimental design of the HNSCC tumorigenesis model and treatment strategy. B. Representative examples of head and neck magnetic resonance imaging (MRI) for different groups. The dashed area is the boundary of the tumor. C. Representative images of 4NQO induced HNSCC (upper) and corresponding HE staining (lower) (left). Quantification of SCC number (upper) and tongue lesion area (lower) (right) in different treatment groups. Scale bar, 1mm (upper), 100μm (lower). P values are presented by one-way ANOVA with Tukey's multiple comparison test. D and E. Representative images of ITGB6 (D), PF4 (E) IHC staining (left) and quantification of percentage of $ITGB6^+$ (D), $PF4^+$ (E) (right) in different treatment groups. Scale bar, 50μm. Data are presented as mean ± SD (n=8). P values are presented by one-way ANOVA with Tukey's multiple comparison test. F.Tumor growth curves for each mouse treated with either the combination of α-PD1 and α-ITGB6 or the control α-PD1 treatment, with measurements recorded every four days. G.Representative images of 4NQO induced HNSCC (upper) and corresponding HE staining(lower). Scale bar, 1mm (upper), 100μm (lower). H and I.Quantification of tongue lesion area (H) and SCC number (I) in different groups. P values were calculated by two-tailed unpaired Student's t-test.

3.The authors acknowledge in the discussion that multiple mechanisms may account for ICI (and α-CD276) resistance. However, all their emphasis on ITGB6 appears to be initiated based on scRNAseq from a single mouse resistant to α-CD276 as

compared to a single mouse whose tumor size was reduced after α-CD276 treatment, and 2 untreated mice controls (line 131). The reviewer appreciates the elegant bioinformatics analysis of this experiment, and yet questions the generality of the prediction of ITGB6 as a resistance mechanism base on the limited sampling. This raise concerns over the rest of the studies.

Response: We thank the reviewer for highlighting this issue. As stated in our manusccript "To search for the systematic biomarkers that respond to α-CD276 treatment, we performed single-cell RNA sequencing (scRNAseq) on samples each pooled from three fresh tissue collected after microdissection, including one resistant, one sensitive and two control pooled samples (Fig. 1E)". We also validated our findings using IHC in control , sensitive and resistance mice (New Figure 2C and D). We consistently detected the upregulation of ITGB6 in pooled scRNAseq and IHC results.

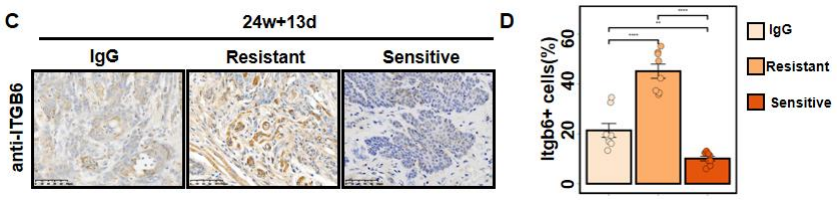

New Figure 2C and D. Representative images of ITGB6 IHC staining (C) and percentage of ITGB6^{+}cells (D) in different treatment groups. Scale bar, 50μm. Data are presented as mean ± SD (n=8). P values are presented by two-tailed unpaired Student's t test.

4.The tumor response is not clearly defined, as most immunotherapy responses are assessed based on complete responses (clinical or histological) in addition to tumor volume changes.

Response: We value your suggestion. In the revised manuscript, we have detailed the outcomes of tumor progression for all treated mice by evaluating three variables: tumor grade, lesion area, and SCC number (New Figure 1D and Figure S1F-H). Below, we present the relevant figures from the manuscript that showcase these assessments.

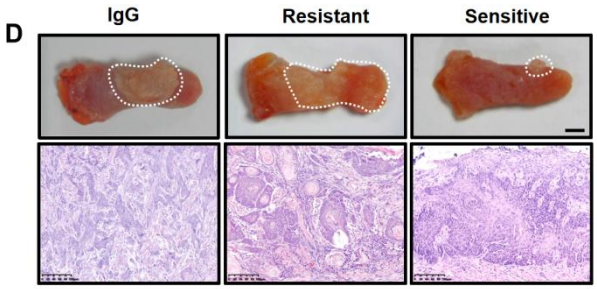

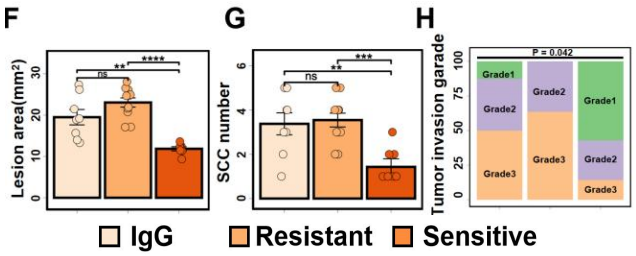

New Figure 1D. Representative images of 4NQO induced HNSCC (upper) and corresponding HE staining(lower). Scale bar, 1mm (upper), 100μm (lower).
New Figure S1F-H. F and G. Quantification of tongue lesion area (F) and SCC number (G) in in different treatment groups. P values were calculated by one-way ANOVA with Tukey's multiple comparison test. H. Quantification of primary tumor incidence in in different treatment groups. P value was calculated by Pearson chi-square test.

5. IHC analysis (e,g., CD8) after 41 days of treatment may reflect more the status of residual disease than relate to the initial antitumoral mechanism (or lack thereof).

Response: We thank the reviewer for their inquiry. In the revised manuscript, we present the results of IHC staining for mice treated with the α-CD276 antibody, captured at three distinct time points: 13 days, 27 days, and 41 days post-treatment (New Figure S1A-E). The following are the pertinent images from the revised manuscript, detailing these results.

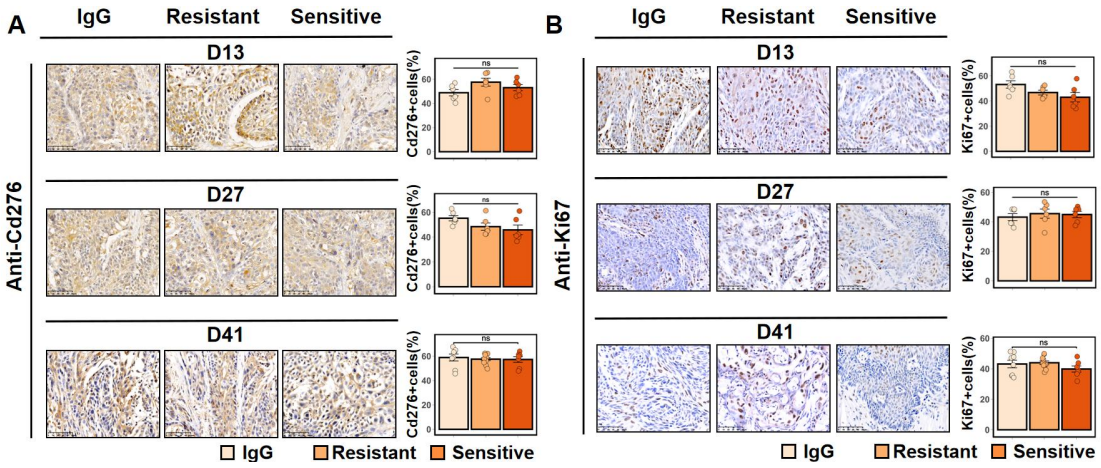

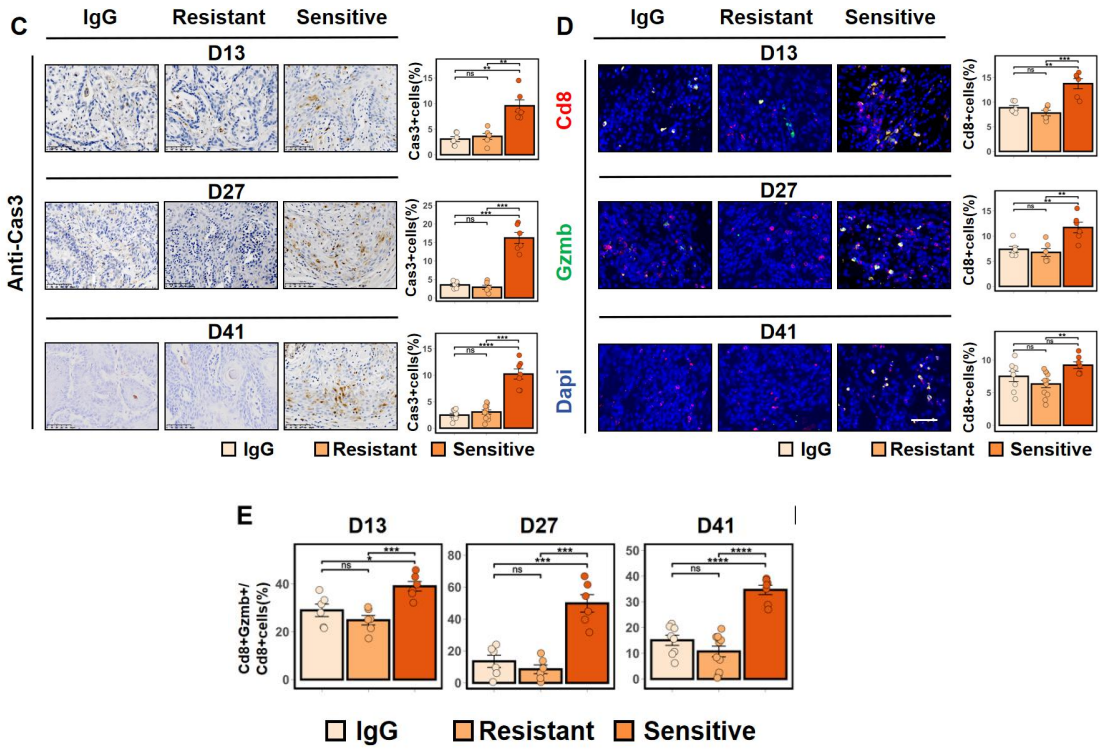

New Figure S1A-E. A-C. Representative images of CD276 (A), KI67 (B), and Caspase-3 (C) IHC staining (left) and quantification of percentage of $CD276^+$ (A), $KI67^+$ (B), and $Caspase\text{-}3^+$ (C) cells (right) in different treatment groups and time points. Scale bar, 100μm. Data are presented as mean ± SD (Day 41 IgG=8, Resistant=11, Sensitive=7, Day 13 and 27 n=6). P values are presented by one-way ANOVA with Tukey's multiple comparison test. D and E. Representative immunofluorescence (IF) staining images of CD8 (green) and GZMB (red) (D). Statistical analysis of the ratio of $CD8^+$ cells and $CD8^+$ $GZMB^+$ cells to $CD8^+$ cells (CD8T killing capacity) (E) in different treatment groups . Scale bar, 25μm. Data are expressed as mean ± SD (Day 41 IgG=8, Resistant=11, Sensitive=7, Day 13 and 27 n=6). P values are presented by one-way ANOVA with Tukey's multiple comparison test.

6. In Figure S1C, it is unclear if active caspase staining is in the tumor or stromal cells.

Response: We extend our gratitude to the reviewer for their recommendation. Concerning the IHC statistics, please note that they were conducted across the entire tumor to ensure comprehensive analysis. To eliminate any ambiguity, we have substituted the original images with more representative ones (New Figure S1C). This modification is intended to offer clearer and more precise visual substantiation of our results.

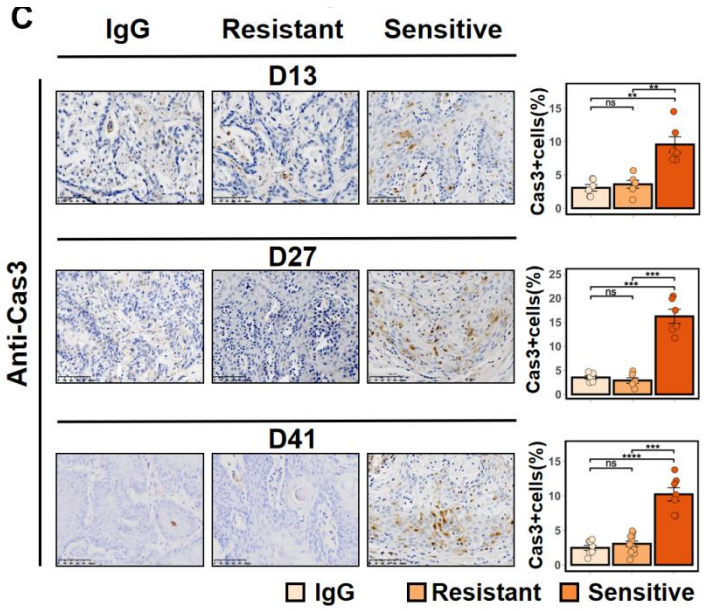

New Figure S1C. Representative images of Caspase-3 IHC staining (left) and quantification of percentage of Caspase-3^{+} cells (right) in different treatment groups . Scale bar, 100μm. Data are presented as mean ± SD (Day 41 IgG=8, Resistant=11, Sensitive=7, Day 13 and 27 n=6). P values are presented by one-way ANOVA with Tukey's multiple comparison test.

7. The use of MOC1 cells (including inoculation site) for validation experiments is not clearly justified.

Response: We appreciate the reviewer's meticulous attention to the details of our experimental setup, particularly the use of MOC1 cells and their specific inoculation site. The selection of MOC1 cells was guided by their established relevance to HNSCC research. These cells represent the unique tumor microenvironment and immune responses characteristic of HNSCC, providing a pertinent model for our studies. Their well-recognized status in HNSCC research facilitates direct comparisons with the existing body of literature.

As for the choice of inoculation site, we initially chose the flank area of trunk for subcutaneous injection. Based on the reviewer's comment, to ensure uniform measurements of tumor growth while replicating the local immune landscape typically associated with HNSCC, we additionally tested our control and knockout cell lines using orthotopic models (New Figure 2A and B). Both strategies showed that ITGB6 plays a greater role in the resistance of a-CD276 treatment. We have added a detailed description of our orthotopic experiments to the Methods section in the revised version.

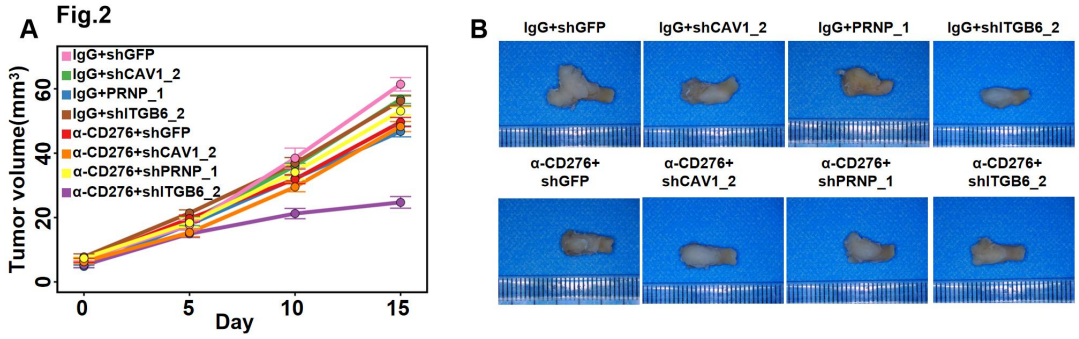

New Figure 2A and B. Growth curves (A) and representative images (B) of HNSCC in mice transplanted in situ in different treatment groups. Data are expressed as mean ± standard deviation (SD) (n=6).

8. Many of the bold statements throughout the study are correlative in nature, and the biological significance of small changes that are barely statistically significant (eg, Fig 2E, Fig 6H and I, Fig 7A and B, Supp Fig 1B) raise also concerns.

Response: We are grateful to the reviewer for their thorough evaluation of the correlations and statistical significances delineated in our study. We recognize that certain outcomes depict only modest variations and border on the brink of statistical significance. This recognition raises legitimate inquiries concerning the biological pertinence of these results. In response, we have amended the manuscript to clarify that, although these changes may seem not as dramatic, they are nonetheless in line with more extensive patterns observed throughout the research. This consistency bolsters the overarching narrative and validates the conclusions drawn from our work. We underline that, while these contributions are nuanced, they incrementally enrich the collective evidence supporting our hypotheses.

9. Limited information is provided about $PF4^{+}$ macrophages and their role in ICI response.

Response: We appreciate your constructive comments and have implemented the suggested revisions in the revised manuscript. Indeed, we had previously recognized the issue mentioned and bred Pf4Cre;DTR mice, which allow us to ablate PF4+ lineage cells upon diphtheria toxin treatment. However, the problem of this mouse model is that we can not exclude the early lineage of PF4 expressing cell, which at the time of toxin treatment could be PF4 negative but still can be depleted. Recognizing this problem, we have ordered a custom Pf4CreERT mouse strain and successfully bred a more stringent Pf4creERT; RosaDTA mouse model. However, challenges associated with the timing of the induction phase prevented our initial manuscript from showcasing pertinent data promptly. Updated results illustrate that tamoxifen treatment markedly reduces PF4+ macrophage levels and augments the response of 4NQO-induced HNSCC mice which are resistant to α-CD276 therapy. New Figure 5E illustrates our strategic approach. Comparative analysis of lesion number, area, and

histopathology indicates that, compared to the control group treated with IgG (Pf4-ctl), the combined treatment with Pf4-ctl and α-CD276 does not significantly inhibit tumor progression (New Figure 5F-I). Conversely, the Pf4-cKO group treated with IgG showed a moderate decrease in tumor growth, a trend that was more pronounced in the Pf4-cKO group treated with α-CD276 (Figures 5F-I).

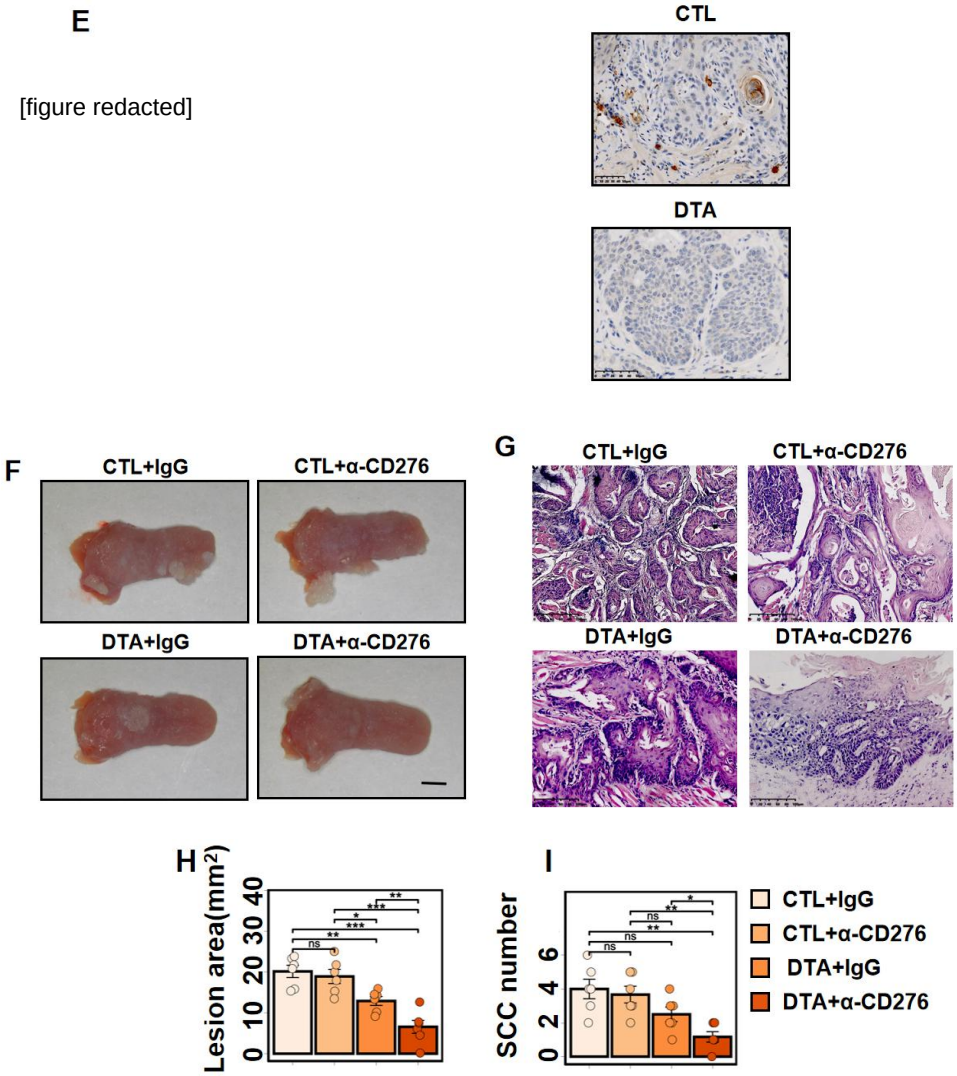

New Figure 5E-I. E. The experimental design of the HNSCC tumorigenesis model and treatment strategy (left) and representative image of PF4 IHC staining in CTL (upper) and DTA (down) groups (right). F. Representative image of 4NQO-induced HNSCC in different groups. Scale bar, 1mm (right). G. Display of histological characteristics of HNSCC in different groups by H&E. Scale bar, 100μm. H and I. Quantification of tongue lesion area (H) and SCC number (I) in in different treatment groups. P values were calculated by one-way ANOVA with Tukey's multiple comparison test.

Reviewer #2

In this study Caihua Zhang et al, explore the cellular and molecular cues underlying resistance to anti-CD276 based-immunotherapy in murine models of Head and Neck cancer. They find that ITBG6 expressed by tumors is responsible of their resistance to

aCD276 treatment. ITGB6 controls CX3CL1 release by the tumor and the attraction of $CX3CR1^{+}PF4^{+}$ tumor associated macrophages. These macrophages are able to induce $CXCR6^{+}CD8^{+}$ T cell exhaustion by secreting inhibitory amount of CXCL16. CXCL16 alone is indeed able to promote T cell exhaustion. The study is elegantly conducted and comprise murine genetic models, human relevance and in vitro/in vivo mechanistic experiments. However, additional experiments should be provided to better understand the role of ITGB6 and CXCL16 in T cell exhaustion.

Response: Thank you for your encouraging feedback and constructive suggestions. In accordance with your recommendations, we have thoroughly revised our manuscript. Presented below are our detailed, point-by-point responses alongside the newly added data, which have been incorporated to address your valuable comments effectively.

1-In the induced model: why tumor grow less in KO mice without treatment? Is it T cell mediated? Overall it should be clarified that the reduction in tumor growth after aCD276 treatment of these tumor models (both induced and transplanted) is mediated by CD8 or CD4 T cells. Authors should address this by using anti-CD4 and anti-CD8 depleting Antibodies.

Response: We express our gratitude for your constructive inquiry. Heeding your suggestion, we have carried out supplementary experiments incorporating anti-CD8 and anti-CD4 in conjunction with the CD276 antibody treatment (New Figure S1I-K), as well as in the ITGB6 knockout groups for both induced (New Figure 2I-K) and transplanted (New Figure S3A-C) tumors. Detailed information about the antibodies is now included in the Methods section, and the pertinent images have been integrated into the revised manuscript.

New Figure S1I-K

[figure redacted]

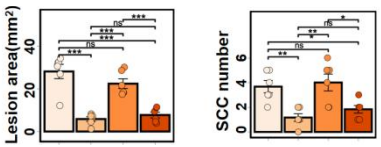

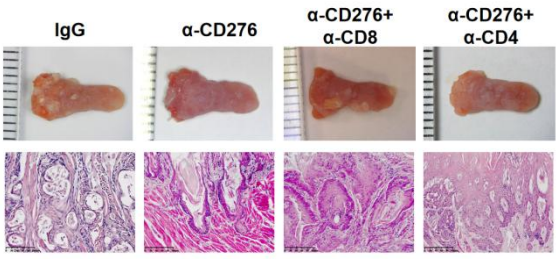

New Figure 2I-K

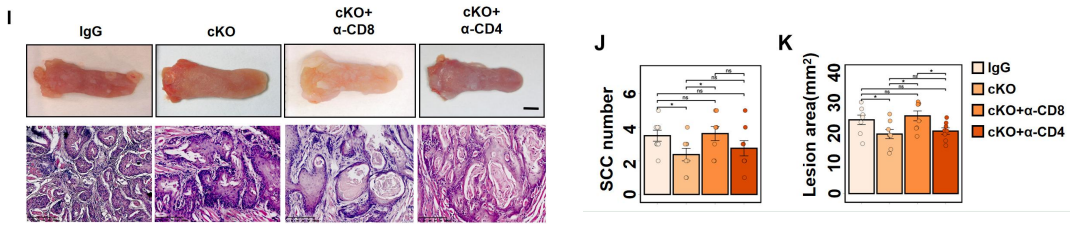

New Figure S3A-C

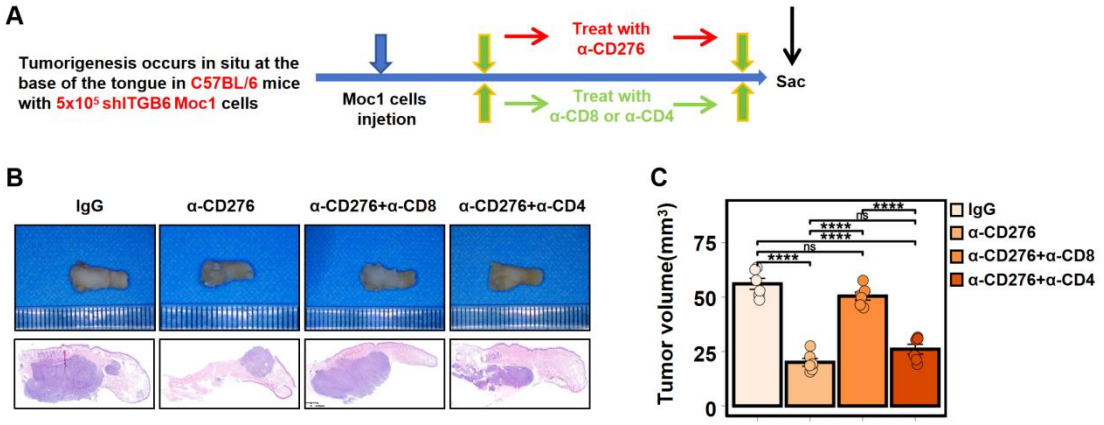

New Figure S1I-K. I.The experimental design of the HNSCC tumorigenesis model and treatment strategy. J. Representative images of 4NQO induced HNSCC (upper) and corresponding HE staining (lower) in different treatment groups. Scale bar, 1mm (upper), 100μm (lower). K. Quantification of tongue lesion area (left) and SCC number (right) in different treatment groups. Data are presented as mean ± SD (n = 6). P values are presented by one-way ANOVA with Tukey's multiple comparison test.

New Figure 2I-K. I. Display of histological characteristics of HNSCC in different groups by H&E (down) and the representative image of 4NQO-induced HNSCC (upper). Scale bar, 100μm (down) and 1mm (upper) . J and K. Quantification of tongue SCC number (J) and lesion area (K) in different treatment groups. Data are presented as mean ± SD (n = 6). P values were calculated by two-tailed unpaired Student's t-test.

New Figure S3A-C. A. Experimental design for the transplantation model and treatment procedure. The C57BL/6 mice, which injected with shITGB6 Moc1 cells, received either α-CD8 or α-CD4 treatment with α-CD276 treatment. B. Representative images of 4NQO induced HNSCC (upper) and corresponding HE staining (down) in different treatment groups. Scale bar, 1mm (upper), 100μm (down). C. Quantification of tumor volume in different treatment groups. Data are presented as mean ± SD (n = 6). P values are presented by one-way ANOVA with Tukey's multiple comparison test.

2-Fig3H : scRNAseq

Authors should clarify how they have identified macrophages versus dendritic cells

Usually macrophages express CSF1R and FCGR1 (CD64) while dendritic cells express FLT3.

Some macrophage cluster resemble DCs: for instance $CCL17^{+}$ Mac could be DCs since DCs are a source of CCL17. Authors should provide the data allowing the reader to identify the clusters.

Another question here: where are type 2 DCs? Type 2 DCs (Mgl2, IRF4) are generally well represented in tumor and often much more abundant than type 1 DCs (Clec9a, IRF8).
Overall, we miss some methodology to fully appreciate the scRNAseq data.

Response: Thank you for addressing this matter. You are correct in highlighting our error: CC17^{+}DCs were mistakenly identified as CCL17^{+}Macrophages due to an oversight. In truth, CC17^{+}DCs are defined by the expression of characteristic genes associated with Type 2 dendritic cells (DCs), whereas Clec9a^{+}DCs are marked by genes typical of Type 1 DCs (New Figure 4H and S5C and D). This clarification is supported by the studies of Bin-Zhi Qian et al. and Zemin Zhang et al. (PMID: 35690521, 33545025), which served as references for our myeloid cell definitions. We have corrected this in the revised manuscript and provided a table featuring the characteristic genes of myeloid cells (Related table1). Attached are the updated images and an excerpt from the table detailing these genes.

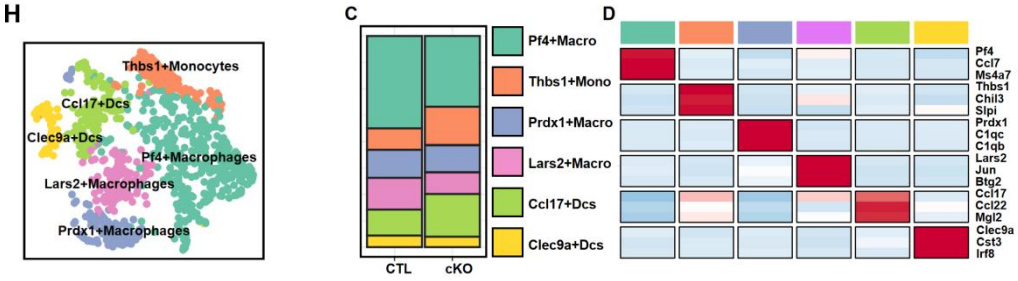

New Figure 4H. UMAP plot of macrophage subpopulation, colored by clustering.
New Figure S5C and D. C. The proportions of MoMΦDC subclusters between the two groups. D. Heatmap of signature genes for MoMΦDC cells subclusters. Each cell cluster is represented by three specifically expressed genes.

Related table1:

p_val	avg_log2FC	pct.1	pct.2	p_val_adj	cluster	gene
3.59E-31	3.292041991	0.315	0.041	3.07E-27	Ccl17+Dcs	Ccl17
2.16E-15	1.243305487	0.525	0.237	1.85E-11	Ccl17+Dcs	Mgl2
9.83E-23	0.851510515	0.716	0.321	8.41E-19	Ccl17+Dcs	Irf4

3-Authors show that ITGB6^{+} tumor recruit PF4^{+} macrophages through a CX3CL1-CX3CR1 axis. This suggest that PF4^{+} macrophages are of monocyte origin and locally recruited upon tumor develoment. If true authors should phenocopy their finding by using an anti-CCL2 or anti-CCR2 antibody.

Response: We express our gratitude for your suggestion. Consistent with your observations, following the application of the CCL2 antibody, there was a notable decrease in both the proportion of PF4^{+} macrophages and the general macrophage population (New Figure S7B). Enclosed are the additional images we have incorporated into the manuscript to visually demonstrate these findings.

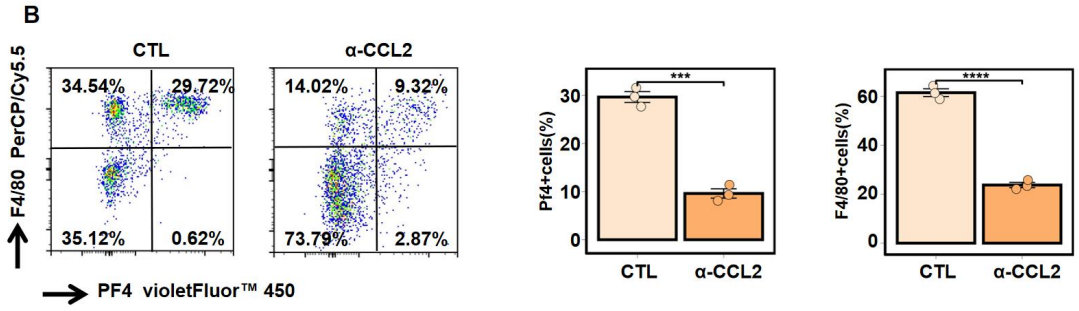

New Figure S7B. Representative flow cytometry plots (left) and statistical analysis of F4/80^{+}PF4^{+} and F4/80^{+} macrophages (right) in different treatment groups. Data are presented as mean±SD (n=3). P value was calculated by two-tailed unpaired Student's t-test.

4- Related to my previous comment: In Fig 5I: authors should quantify the other macrophage subsets. Indeed CX3CR1 is expressed by monocytes and blocking this chemokine receptor should reduce all monocyte-derived macrophage subsets in the tumor.

Response: We are grateful for your inquiry. In response, we have incorporated the pertinent statistical data concerning the proportions of PF4^{+} macrophages and overall macrophage populations into the appropriate sections of our manuscript. Our findings reveal that inhibition of either CX3CL1 or CX3CR1 results in a decreased presence of all macrophage subgroups within the tumor microenvironment (New Figure 6L and M).

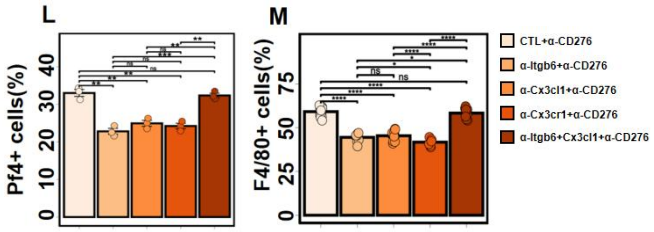

New Figure 6L and M. L. Quantification of the proportions of F4/80^{+}PF4^{+}cells in different treatment groups. P values are presented by one-way ANOVA with Tukey's multiple comparison test. M. Representative flow plots show frequency of the F4/80^{+} macrophages in different treatment groups. P values are presented by one-way ANOVA with Tukey's multiple comparison test.

4-Authors switch from their elegant K14-ITGB6fl model to the use of an anti-ITGB6

antibody? This new model of ITGB6 inhibition is not well documented. Can this Ab directly kill tumor cells? Would be important to show a reduction in CX3CL1 and CXCL16 in anti-ITGB6 treated mice.

Response: We value the reviewer's inquiries concerning the anti-ITGB6 antibody (264RAD). According to existing research, particularly in colorectal and breast cancer models, the primary mechanism of the anti-ITGB6 antibody does not involve direct killing of tumor cells. Rather, its effectiveness is predominantly observed in altering the tumor microenvironment, with a notable influence on T-cell responses. Specifically, the blockade of integrin αvβ6, targeted by the anti-ITGB6 antibody, is reported to bolster T-cell-mediated tumor immunity, leading to tumor regression, particularly when combined with PD-1 inhibitory treatments (PMID: 35131862, 33385331). To determine whether 264RAD mirrors the in vivo suppressive effects of ITGB6 on CX3CL1 and CXCL16 expression, we performed Western blot analyses. These experiments demonstrated that 264RAD markedly reduced the expression levels of CX3CL1 and CXCL16 in the treated mice (New Figure S7O).

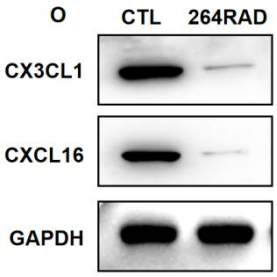

New Figure S7O. Western blotting analysis of CX3CL1 and CXCL16 in control and 264RAD-treated mice.

5-On the T cell side, authors do not discriminate $CD4^+$ T conventional cells from $CD4^+$ Treg cells. Tregs are key immunosupressive cells in tumors and their functionality is regulated by TGFb, which is itself regulated by ITGB6. Authors should provide data showing no impact of the loss of ITGB6 on Tregs.

Response: Thank you for your insightful suggestion. Heeding your guidance, we have refined our analysis by further categorizing CD4 T cells into CD4 TH and Tregs in our single-cell datasets (New Figure 4F and S5B). Analysis of the cellular proportions revealed no substantial variations in Treg proportions between the CTL group and the ITGB6 cKO group (New Figure S4K and L). Expanding on this, we employed flow cytometry to investigate Treg dynamics specifically during ITGB6 gene ablation and subsequent to combined ITGB6 knockout and α-CD276 treatment (New Figure S5N and O). These studies affirmed that ITGB6 deletion does not significantly impact Treg infiltration. Below, we display the pertinent images from our manuscript illustrating these findings.

New Figure 4F and S5B

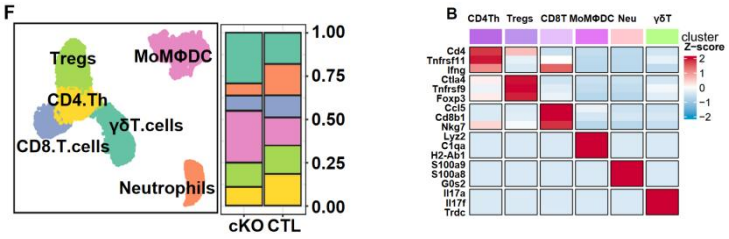

New Figure S4K and L

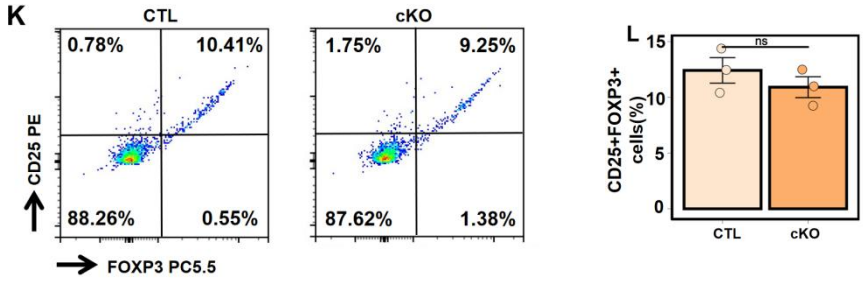

New Figure S5N and O

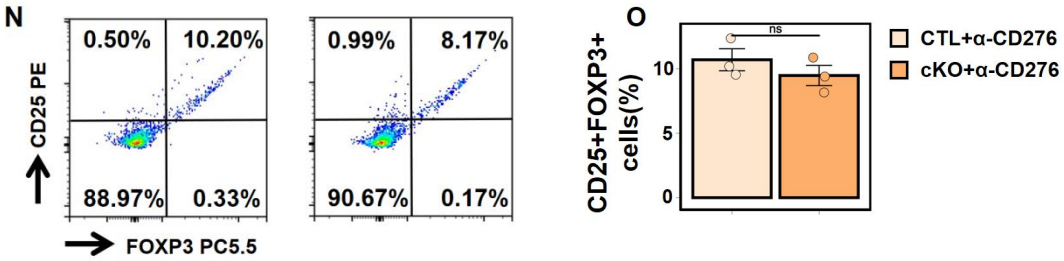

New Figure 4F. The UMAP diagram of the immune cell subpopulation (left) and the cell ratio between the two groups (right).

New Figure S5B. Heatmap of signature genes for Immune cells subclusters from mouse HNSCC tumor tissues. Each cell cluster is represented by three specifically expressed genes.

New Figure S4K and L . Representative flow plots show frequency of Tregs (K) and quantification of the proportions of Tregs (L) in CTL and cKO mice. P values were calculated by two-tailed unpaired Student's t-test.

New Figure S5N and O. Representative flow plots show frequency of Tregs (N) and quantification of the proportions of Tregs (O) in different treatment groups. P values were calculated by two-tailed unpaired Student's t-test.

6-A novel and surprising finding is the direct role of CXCL16 in the exhaustion of T cells. Is CXCR6 a signaling receptor? To better understand how this chemokine functionnaly impacts T cell differentiation authors should show how CXCL16 impacts T cell states at the transcriptomic level like it has been done for $PF4^{+}$ macrophages (FigS9)

Response: We extend our gratitude for your valuable suggestion for revision. In

accordance with your recommendation, we have enhanced our revised manuscript with the appropriate analyses and experiments. To further assess the influence of the CXCR6 receptor on $CD8^+$ T cell functionality and state, a differential gene expression analysis was carried out. The results revealed that the $GZMB^+$ $CXCR6^+$ $CD8^+$ T cell subgroup was predominantly enriched in pathways associated with the immune response and antigen processing and presentation, indicative of immune activation. Conversely, the $PDCD1^+$ $CXCR6^+$ $CD8^+$ T cell group displayed greater enrichment in lectin C and glycolysis pathways (Fig. S11A and B). A subsequent SCENIC analysis showed that CREM gene expression was significantly elevated in the $PDCD1^+$ $CXCR6^+$ $CD8^+$ T cell group (Fig. S11C). To further determine CREM's role in $CD8^+$ T cell depletion, SCENIC analysis was applied to $CD8^+$ T cells data from Robert L. Ferris et al., confirming high CREM activity in the $PDCD1^+$ $CXCR6^+$ $CD8^+$ T cell subgroup (Fig. S11D). To explore the possibility that CREM activity in this group is regulated by the CXCL16-CXCR6 axis, $CD8^+$ T cells were isolated from tumor tissues and subjected to activation with 100ng/ml and 800ng/ml concentrations of CXCL16 recombinant protein (Fig. S11E). Findings indicated that the low CXCL16 concentration group showed a significant decrease in the $PDCD1^+$ $CXCR6^+$ $CD8^+$ T cell fraction and an increase in the $GZMB^+$ $CXCR6^+$ $CD8^+$ T cell fraction compared to the high concentration group (Fig. S11F and G). Western blot analyses on sorted $PDCD1^+$ $CXCR6^+$ $CD8^+$ T and $GZMB^+$ $CXCR6^+$ $CD8^+$ T cells demonstrated a notable increase in CREM levels within the $GZMB^+$ $CXCR6^+$ $CD8^+$ T cell subgroup, suggesting that CREM may mediate the exhaustion process in $CXCR6^+$ $CD8^+$ T cells (Fig. S11H).

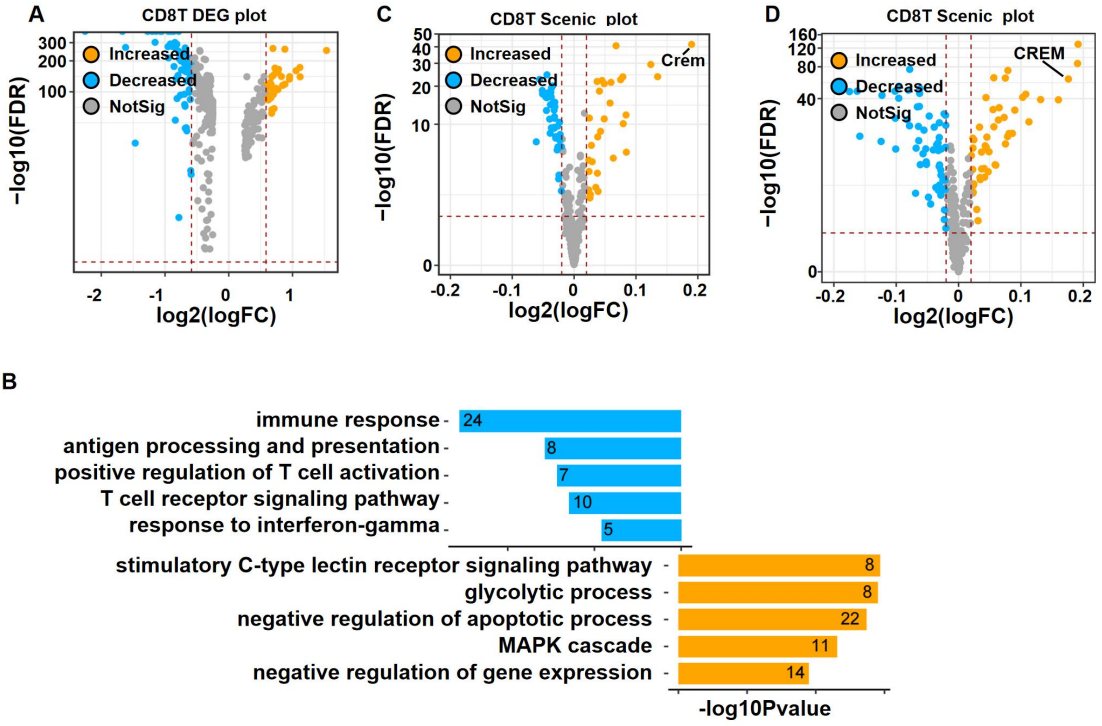

[figure redacted]

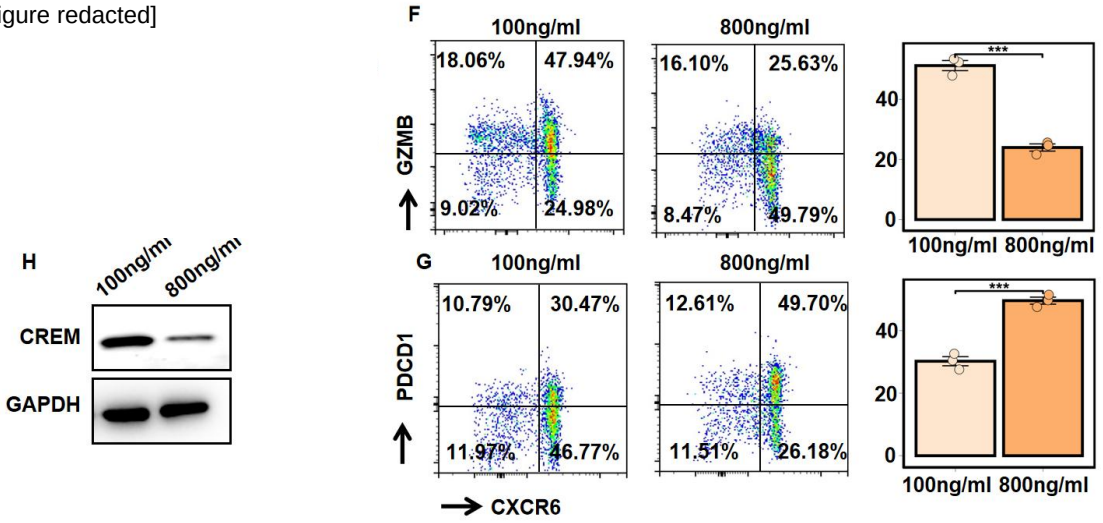

New Figure S11. A. Differential expression analysis identifies differences in GZMB$^+$CXCR6$^+$CD8$^+$T cells and PDCD1$^+$CXCR6$^+$CD8$^+$T cells. Differential expression analysis by DEseq2. Volcano plots demonstrating significant ($p<0.05$) differential ($|logFC|>0.585$) abundances. B. GO pathway enrichment analysis of differentially expressed genes of CD8$^+$T cells in different subsets. C. Volcano plot showing differences in transcription factors of CD8$^+$T cells between the two subsets, transcription factors derived from Scenic analysis. D. Volcano plot showing differences in transcription factors of CD8$^+$T cells between the two subsets in data from Robert L. Ferris et al, transcription factors derived from Scenic analysis. E. The experimental design of T cell killing experiments. F. Representative flow plots show frequency of the CXCR6$^+$ CD8$^+$ GZMB$^+$ T cells (left) and quantification of the proportions of CXCR6$^+$ CD8$^+$ GZMB$^+$ T cells (right) in groups different CXCL16 doses. P values were calculated by two-tailed unpaired Student's t-test. G. Representative flow plots show frequency of the CXCR6$^+$ CD8$^+$ PDCD1$^+$ T cells (left) and quantification of the proportions of CXCR6$^+$ CD8$^+$ PDCD1$^+$ T cells (right) in groups different CXCL16 doses. P values were calculated by two-tailed unpaired Student's t-test. H. Western blotting analysis of CREM in different subsets of CXCR6$^+$CD8$^+$T cells.

Minor comments

1- "Before aCD276 treatment, mice are selected in the wt and ko group for similar lesion size." This should be documented. (line 204)

Response: Thank you for emphasizing the significance of thorough documentation. We recognize this lapse and have subsequently incorporated the pertinent data into the revised manuscript.

2- Missing stats in figure 2F (tumor growth curves)

Response: We value your scrutiny regarding the omitted statistical details in Figure 2F.

We have rectified this by incorporating the appropriate statistical analyses for the tumor growth curves, thereby ensuring that our findings are represented clearly and accurately (New Figure 3A).

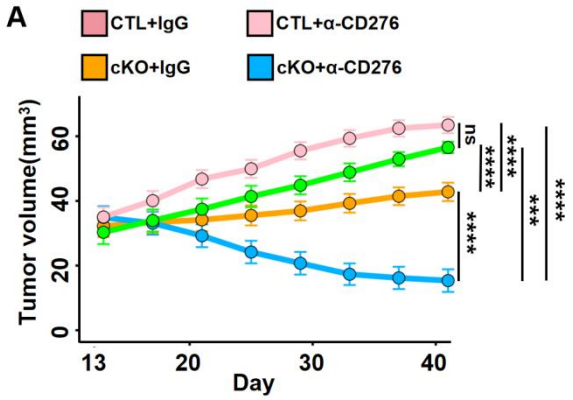

New Figure 3A.The tumor growth curves of different groups of mice were plotted. Measurements were taken every 4 days. P values were calculated by one-way ANOVA and Tukey HSD test.

3- In S4C: Clec9^{+} cells are mark as “Macrophages” in the bar plot but are “DCs” in the UMAP of Fig3H

Response: We apologize for the confusion stemming from the mislabeling in Figure S4C. You are correct; Clec9^{+} cells should indeed be classified as dendritic cells (DCs), not macrophages. This error has been corrected in the revised figure to accurately represent the data depicted in the UMAP.

4- Missing color code in figure 3I for the connecting lines

Response: Thank you for highlighting the omission of the color code in Figure 3I. The oversight was unintentional, and we have now rectified this in the updated version of the figure (New Figure 4I).

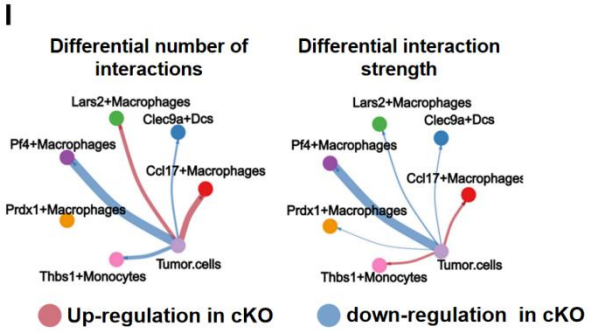

New Figure 4I. Circle plot showing the differences in the number and strength of intercellular communications between the two groups by CellChat. Both the strength and number of intercellular communications between PF4^{+} macro and tumor cells were significantly reduced. (The blue line represents intercellular communication

down-regulation, red represents up-regulation, and the width of the line represents the number of up- or down-regulation).

5- Fig 6D: “Suppressive” is not correct to refer to T cell state. Authors should say “suppressed” or better “terminally exhausted” (=co expressing several inhibitory receptors)

Response: We express our gratitude for your feedback regarding the terminology employed in Figure 6D. We have revised the term to 'suppressed' to more precisely denote the state of T cells exhibiting multiple inhibitory receptors, aligning with contemporary scientific insights.

Reviewer #3

The authors identified ITGB6 expression as essential for resistance of anti-CD276 treatment in mouse HNSCC. They show that while Itgb6 ablation partially mitigates tumor progression, the combination of Itgb6 knockout and α-CD276 treatment leads to a reduction of tumor size. They also propose that ITGB6 mediates the interaction between tumor cells and $PF4^+$ macrophages by CX3CL1-CX3CR1 axis, with $PF4^+$ macrophages contributing to exhaustion in $CXCR6^+CD8^+$ T cells. Finally, they show that signature of $PF4^+$ macrophages is associated with clinicopathological parameters in HNSCC. While the discovery of ITGB6 expression as essential for resistance of anti-CD276 treatment in mouse HNSCC is interesting, the rest of the data presented are not novel and need to be align with current literature.

We are grateful for your recognition of the role of ITGB6 in mediating resistance to anti-CD276 treatment in mouse models of HNSCC. Heeding your guidance, we have meticulously updated the manuscript to better correspond with the contemporary literature, with a special emphasis on delineating the distinctive aspects of our research on ITGB6 and resistance to anti-CD276 therapy in HNSCC. We have revised pertinent sections to incorporate recent studies, thereby clarifying the innovation and importance of our findings in the wider context of existing research. These modifications aim to ensure that the unique contributions of our study are both clear and properly contextualized within the current scientific discourse.

1.No mechanistic data is provided on the role of ITGB6 and why it is essential to resistance of anti-CD276 treatment in mouse HNSCC.

Response: Thank you for your inquiry. In response to your suggestion, we have investigated the role of ITGB6 in functional assays involving HNSCC cell lines. The CRISPR-Cas9 system was employed to knock out ITGB6 in HNSCC cells with high ITGB6 expression (SCC15 cell line: sgGFP, sgITGB6-1, sgITGB6-2), as depicted in Fig. S3D. Following the deletion of ITGB6, the expression of CD276 protein was assessed, and the results indicated that the knockout of ITGB6 did not alter the expression of CD276 protein (Fig. S3D). Experiments examining cell proliferation

and clonogenicity suggest that the knockout of ITGB6 has no significant effect on the proliferation or colony-forming capabilities of HNSCC cells (Fig. S3E and F). Moreover, when compared to the sgGFP control cells, the migration and invasion capabilities of ITGB6 gene knockout cells showed no significant changes (Fig. S3G and H). Concurrently, flow cytometry was utilized to examine the apoptosis levels of ITGB6 gene knockout and control HNSCC cells, revealing that ITGB6 gene knockout did not impact the apoptosis levels of HNSCC cells (Figure. S3I). In summary, these data support the conclusion that ITGB6 does not have a direct impact on the progression of HNSCC. Additionally, we examined the impact of ITGB6 on tumor progression in mouse models, discovering that ITGB6 knockout leads to reduced tumor growth in vivo. Our study further evaluates the role of ITGB6 in immune cell infiltration, indicating that while ITGB6 does not alter Tregs presence (Fig. S4K and L), it significantly impacts $CD8^+$ T cell infiltration (Fig. 2F).

To further validate the aforementioned results, the mice from the ITGB6-cKO group were randomly divided into four groups and treated with anti-CD4 and anti-CD8 depleting antibodies (Fig. 2I). Histological analyses revealed that depleting $CD8^+$ T cells significantly reversed the aggressive growth inhibition mediated by anti-CD276, while depleting $CD4^+$ T cells did not exhibit any impact on the aggressive growth inhibition mediated by anti-CD276 (Fig. 2J). According to the analysis of the overall lesion quantity and area, the depletion of $CD8^+$ T cells significantly weakened the tumor growth inhibition mediated by CD276 blockade, whereas the depletion of $CD4^+$ T cells demonstrated no effect (Fig. 2J and K).

New Figure S3D-I

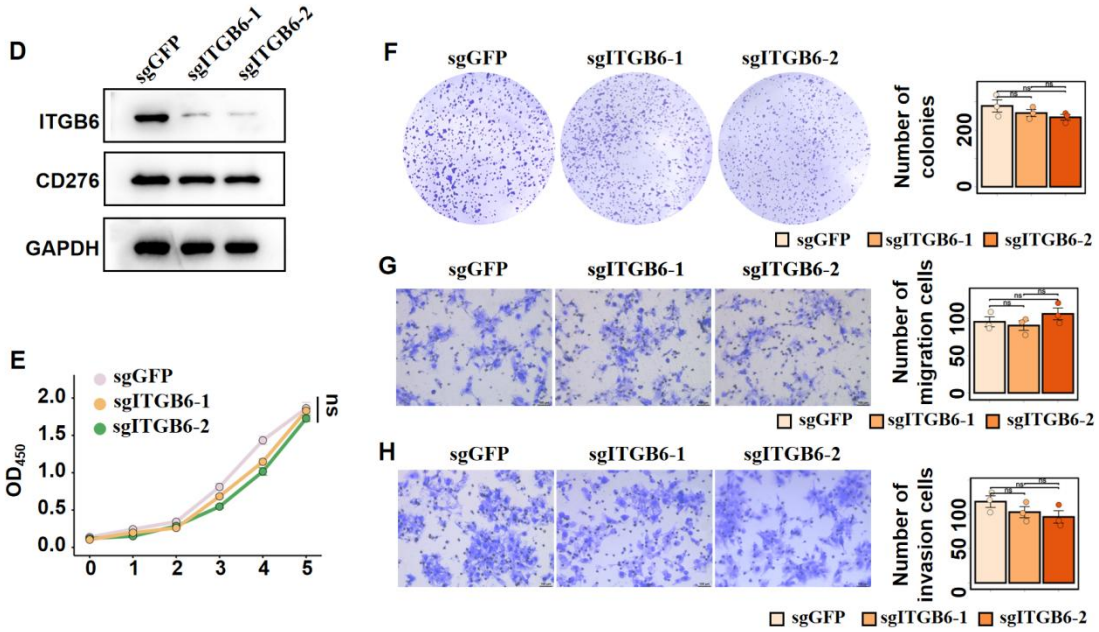

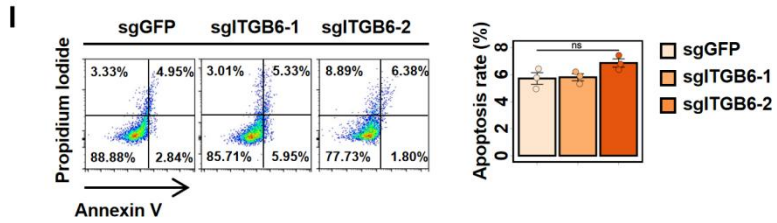

New Figure 2F

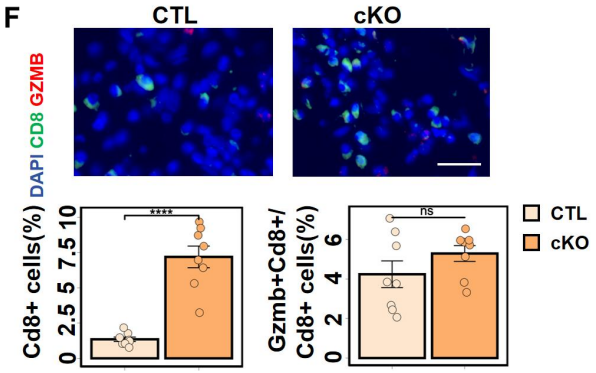

New Figure S4K-L

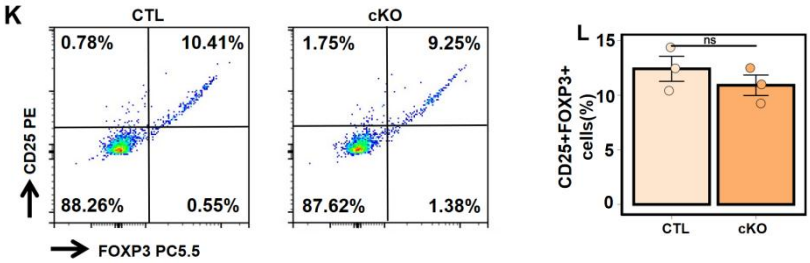

New Figure 2I-K

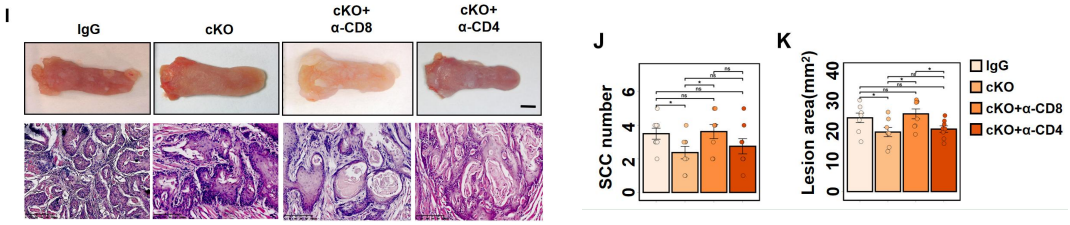

New Figure S3D-I. D.Western blot of ITGB6 and CD276 in ITGB6 KO and control HNSCC cells. E.CCK8 assay of cell proliferation in ITGB6 KO and control HNSCC cells (n = 3). F. Representative images (left) and quantitative analysis (right) of colony formation in ITGB6 KO and control HNSCC cells. G. Representative images (left) and quantitative analysis (right) of Transwell migration in ITGB6 KO and control HNSCC cells. Scale bar, 100 mm. H. Representative images (left) and quantitative analysis (right) of Transwell invasion in ITGB6 KO and control HNSCC cells. Scale bar, 100 mm. I. Representative images (left) and quantitative analysis (right) of apoptosis in ITGB6 KO and control HNSCC cells.

New Figure 2F. Representative immunofluorescence (IF) staining images of CD8 (green) and GZMB (red) (upper). Statistical analysis of the ratio of $CD8^+$ cells and

$CD8^+$ $GZMB^+$ cells to $CD8^+$ cells (CD8T killing capacity) in different treatment groups (down). Scale bar, 25μm. Data are expressed as mean ± SD (n=8). P values were calculated by two-tailed unpaired Student's t test.
New Figure S4K-L. Representative flow plots show frequency of Tregs (K) and quantification of the proportions of Tregs (L) in CTL and cKO mice. P values were calculated by two-tailed unpaired Student's t-test.
New Figure 2I-K. I. Display of histological characteristics of HNSCC in different groups by H&E (down) and the representative image of 4NQO-induced HNSCC (upper). Scale bar, 100μm (down) and 1mm (upper) . J and K. Quantification of tongue SCC number (K) and lesion area (L) in different treatment groups. Data are presented as mean ± SD (n = 6). P values were calculated by two-tailed unpaired Student's t-test.

2.The main issue here is on the nature of $PF4^+$ macrophages. The authors chose to named them based on their expression of PF4. However multiple studies have addressed TAM heterogeneity and this should be added in the context of this study. Especially that the authors have derived a distinct gene signature for these cells using single-cell RNA sequencing, they should look in others studies to what TAM populations they correspond. Authors should consider compared their data to the recent paper of Pittet laboratory (PMID: 37535729).

Response: Thank you for your profound insights regarding the characterization of $PF4^+$ macrophages. We acknowledge the critical necessity of precisely framing our discoveries within the broader spectrum of tumor-associated macrophage (TAM) heterogeneity. To this end, we have amended the manuscript to provide a thorough discussion on the diversity of TAMs, underpinning our discourse with a variety of studies to juxtapose our identified $PF4^+$ macrophage gene signature against TAM populations characterized in other investigations. We have included the full tables of differential gene expression for our delineated myeloid cell subsets. Furthermore, we have executed an in-depth comparison of our myeloid cell groups against established benchmarks in the field. The analyses confirm that the gene expression profiles of $Clec9a^+$ Dcs and $Ccl17^+$ Dcs correlate with those of Type 1 and Type 2 dendritic cells, respectively, whereas $Thbs1^+$Monocytes display gene signatures similar to classical tumor-infiltrating monocytes. Our $PF4^+$ macrophages manifest traits analogous to both immune regulatory TAMs and megakaryocytes. Conversely, $Prdx1^+$ Macrophages and $Lars2^+$ Macrophages resemble lipid-associated and inflammatory cytokine-rich TAMs, respectively. Heeding your advice, we have also juxtaposed our findings on $PF4^+$ macrophages against the macrophage polarization described by CXCL9 and SPP1 in Pittet's study, enriching our comprehension of TAM heterogeneity and positioned our findings within the broader context of global research.

3.The notion that TAM contributed to exhaustion of $CD8^+$ T cells is not novel.

Response: Thank you for your constructive comments. We recognize that numerous studies have documented the role of tumor-associated macrophages (TAMs) in promoting $CD8^+$ T cell exhaustion. However, the specific impact of PF4 has been predominantly examined in contexts such as its influence on Spp1 macrophage differentiation and fibrosis post-heart and kidney injuries (PMID:36807143), its effects on monocytes and monocyte-derived cells (28899579, 2275902), its initiation of signaling cascades and downstream epigenetic reprogramming via CXCL4 affecting cytokine expression (35701499), and its role in innate immunity through macrophage activity (32846949). Concerning $PF4^+$ macrophages, reports have largely covered their involvement in angiogenesis promotion (28978662) and their M2-like characteristics (38167034). Their specific regulatory functions within the tumor immune microenvironment, however, demand further detailed exploration.

Recent studies have highlighted the unique expression of CXCR6 on intratumoral $CD8^+$ T cells, underscoring their enhanced immunocompetence and pivotal role in antitumor activity. Contrarily, $CD8^+$ T cells devoid of chimeric receptors exhibit diminished antitumor efficacy. Notably, Cxcr6-/- mice exhibit a compromised response to PD-1 treatment, indicating the crucial role of $CXCR6^+CD8^+$ T cells in augmenting the effectiveness of anti-PD-1 therapies and thereby decelerating tumor growth (PMID: 34462326). Further research corroborates that the absence of CXCR6 or disruption of its interaction with its ligand compromises the tumor control exerted by $CD8^+$ T cells. Additionally, CXCR6 has been identified as a predictive marker for the responsiveness of various cancers to immunotherapies targeting PD-(L)1 (36311728). It serves as an indicator for resident memory $CD8^+$ T cells within the tumor, with a lack of CXCR6 leading to diminished retention and consequently, inadequate tumor suppression (33692218, 34607898). Another investigation has defined $CXCR6^+$CD8 T cells as tumor-enriched cells that could act as predictive indicators for high immune infiltration and improved responses to immune checkpoint inhibitors, thus positioning them as potential therapeutic targets (37593098). Despite these significant findings, the detailed regulatory mechanisms and therapeutic implications of $CXCR6^+CD8^+$T cells within the tumor milieu and their precise impact on immunotherapy outcomes are still to be fully clarified.

In our manuscript, we have sought to delineate the unique mechanisms by which $PF4^+$ macrophages, particularly through their interactions with ITGB6, contribute to the exhaustion of tumor-specific $CXCR6^+CD8^+$ T cells, leading to the ineffectiveness of immunotherapy in HNSCC—a novel aspect not yet explored in the literature. Our research highlights the pivotal role and mechanism of the ITGB6-$PF4^+$ macrophage-$CXCR6^+CD8^+$ T cell axis in the context of cancer immunotherapy.

4.The data showing that signature of $PF4^+$ macrophages is associated with clinicopathological parameters in HNSCC is not convincing. In addition it is well described that TAM are protumoral.

Response: Thank you for your inquiry. We have uploaded the code pertaining to the $PF4^+$ related characteristic gene set and conducted survival analyses across multiple

datasets. And in the updated version of our manuscript, we delve into the pivotal function of $PF4^+$ macrophages in mediating resistance to α-CD276 therapy. We developed Pf4creERT; RosaDTA mice for inducing HNSCC, and updated results illustrate that tamoxifen treatment markedly reduces PF4+ macrophage levels and augments the response of 4NQO-induced HNSCC mice to α-CD276 therapy. New Figure 5E illustrates our strategic approach. Comparative analysis of lesion number, area, and histopathology indicates that, compared to the control group treated with IgG (Pf4-ctl), the combined treatment with Pf4-ctl and α-CD276 does not significantly inhibit tumor progression (New Figure 5F-I). Conversely, the Pf4-cKO group treated with IgG showed a moderate decrease in tumor growth, a trend that was more pronounced in the Pf4-cKO group treated with α-CD276 (Figures 5F-I). Our objective was to explore the role of PF4+ macrophages in drug resistance and elucidate the underlying mechanisms, while the prevailing literature on $PF4^+$ macrophages generally centers around their roles in fibrosis, secretion of inflammatory factors, and differentiation from monocytes, with limited exploration into their involvement in immunotherapy resistance and $CXCR6^+CD8^+$ T cell modulation (PMID: 36807143, 28899579, 3570149, 32846949, 37965262). Our study contributes a novel perspective to the understanding of $PF4^+$ macrophages in the context of tumor immunity and $CD8^+$ T cell dynamics.

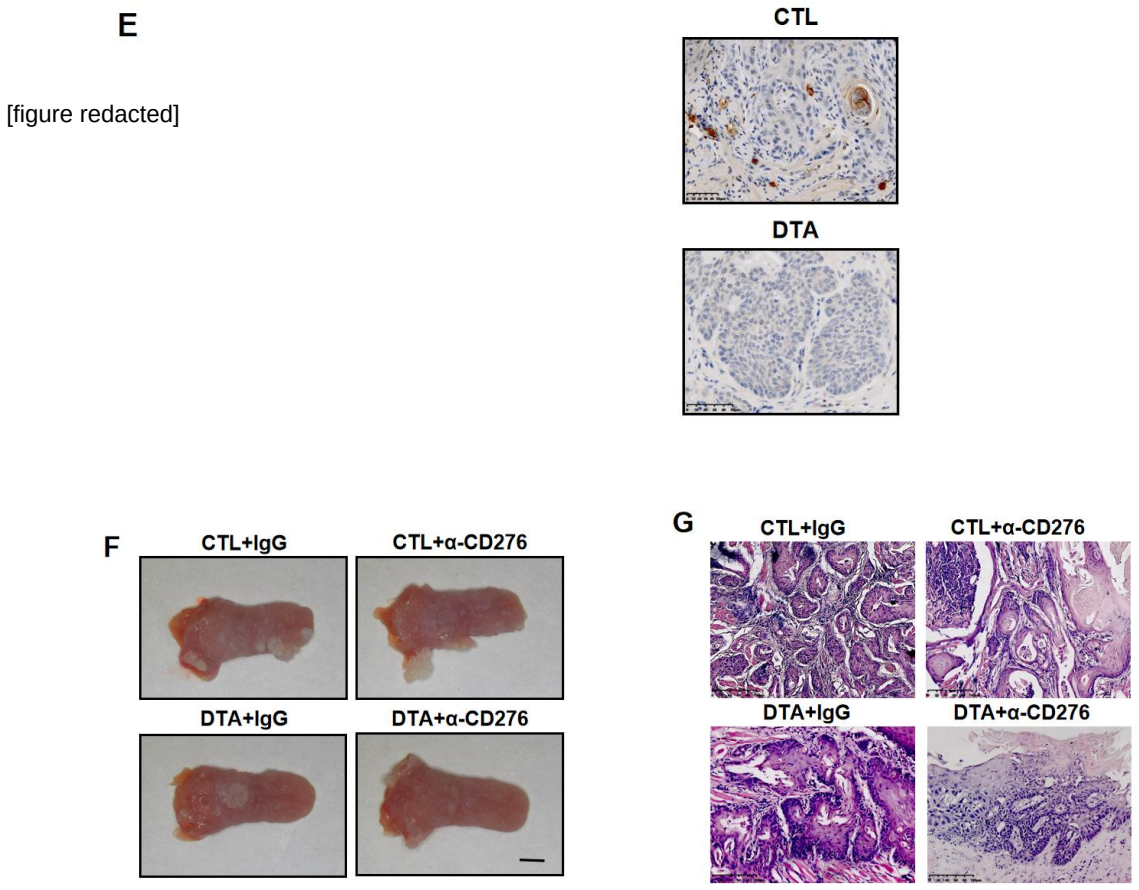

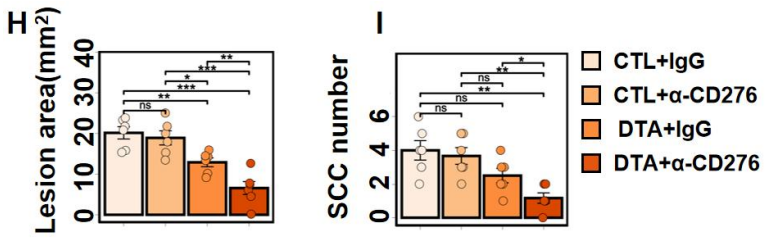

New Figure 5E-I. E. The experimental design of the HNSCC tumorigenesis model and treatment strategy (left) and representative image of PF4 IHC staining in CTL (upper) and DTR (down) groups (right). F. Representative image of 4NQO-induced HNSCC in different groups. Scale bar, 1mm (right). G. Display of histological characteristics of HNSCC in different groups by H&E. Scale bar, 100μm. H and I. Quantification of tongue lesion area (H) and SCC number (I) in in different treatment groups. P values were calculated by one-way ANOVA with Tukey's multiple comparison test.

Reviewer #4 (Remarks to the Author):
This research identifies ITGB6 as a key factor in Enoblituzumab α-CD276 treatment, revealing its role in regulating the expression of CX3CL1 and recruiting $PF4^{+}$ macrophages, suggesting ITGB6 may be a potential target to overcome resistance in Head and Neck Cancer therapy. This manuscript has some interesting findings but also has many problems. The research design needs to be more stringent, and several important issues need to be clarified.

Thank you for your constructive feedback. We fully acknowledge the significance of a rigorous research framework and understand the concerns highlighted. We are dedicated to rectifying these issues and will refine our manuscript to eliminate ambiguities and strengthen the research design. In particular, we will elaborate on our methodology with greater precision, implement robust experimental controls, and elucidate the implications of our findings more clearly. Your insights are highly valued, and we are committed to enhancing the quality of our study.

1.Although the manuscript centers on CD276 therapy, there is not a single figure dedicated to CD276. What is the relationship between CD276 and ITGB6? Does ITGB6 expression correlate with CD276 expression in patient samples? Does ITGB6 regulate Cd276 expression and/or activity?

Response: Thank you for your insightful comments. In alignment with your recommendations, we have expanded our revised manuscript with additional analyses. We assessed the immunohistochemistry (IHC) scores for CD276 and ITGB6 across control, resistant, and sensitive groups at three distinct time points, involving a total of 62 mouse samples. Our findings indicate a notable decrease in ITGB6 IHC scores within the sensitive group compared to the other groups, yet no significant variance was observed in the IHC scores for CD276 between the groups (New Figure S2H-J).

Furthermore, in our studies using HNSCC cell lines, we performed ITGB6 knockouts and employed Western Blot analysis to evaluate CD276 expression levels, which confirmed that ITGB6 ablation does not impact CD276 expression (New Figure S3D). Additional validation was carried out on a set of 81 FAH patient samples, examining the IHC scores for CD276, ITGB6, and PF4. The results affirmed a significant link between ITGB6 and PF4 IHC scores, aligning with our single-cell observations, whereas CD276 scores did not correlate with either ITGB6 or PF4. These results underscore the lack of a direct relationship between ITGB6 and CD276 expressions (New Figure 5J-N). Instead, our data indicate that ITGB6 contributes to the exhaustion of $CXCR6^{+}CD8^{+}$ T cells via $PF4^{+}$ macrophages, thus leading to resistance against α-CD276 antibody treatment. Notably, the isolated suppression of ITGB6 or $PF4^{+}$ macrophages resulted in only partial inhibition of tumor growth, resonating with existing literature suggesting that HNSCC tumor stem cells may circumvent $CD8^{+}$ T cell-mediated destruction through CD276, thus potentially advancing malignant tumor progression.

New Figure S2H-J

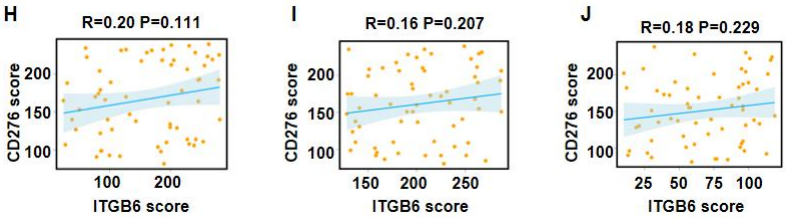

New Figure S3D

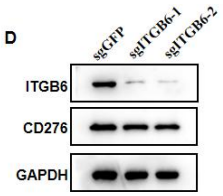

New Figure 5J-N

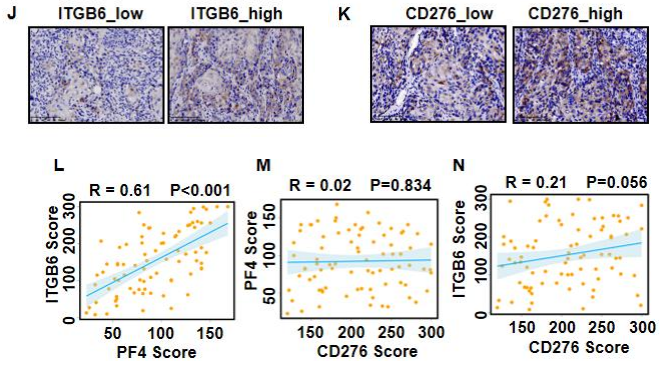

New Figure S2H-J. Correlation of ITGB6 score with CD276 score in IgG, Resistant and Sensitive groups (n=62). P values were calculated by Pearson's correlation analysis.

New Figure S3D. Western blot of ITGB6 and CD276 in ITGB6 KO and control HNSCC cells.

New Figure 5J-N. J. ChIP-qPCR analysis of Stat3 binding to CX3CL1. Data were presented as mean ± SD (n=3). P values were calculated by two-tailed unpaired Student's t-test. K. Western blotting analysis of ERK1/2, SAPK/JNK, PI3K, AKT, FAK, P38 MAPK, NFKB1, STAT3 and analysis of phosphorylated ERK1/2, SAPK/JNK, PI3K, AKT, FAK, P38 MAPK, NFKB1, STAT3 in control and cKO Moc1 cells. L. Violin plot showing the expression of Cx3cr1 in all cell types. M. Immunofluorescence staining to detect expression of mice CX3CR1 (red), and PF4 (green) . DAPI was used for nuclear staining. Scale bar, 25 μm. N. Representative flow plots show frequency of Tregs (upper) and quantification of the proportions of Tregs (down) in different treatment groups. P values were calculated by two-tailed unpaired Student's t-test.

2.Figure 2F requires clarification on how to explain tumors treated with CTL+CD276 grow faster than CTL^{+}IgG-treated tumors. Ensure statistical analysis is performed on Figure 2 data and clearly stated in the figure.

Response: Thank you for addressing this point. The observed variations in tumor volumes among the mice post-induction reflect individual biological differences, leading to the disparities in final volumes depicted in Figure 2F. To rigorously analyze these discrepancies, we computed the tumor growth rate for each individual mouse before employing ANOVA to assess differences between groups. Should ANOVA reveal significant disparities, we subsequently conducted the Tukey HSD test for detailed pairwise comparisons. This analytical approach allows us to evaluate and compare trends in tumor growth rates or other relevant biomarkers over time across different treatment conditions. Our analysis indicated no substantial difference between the CTL+CD276 and CTL+IgG-treated groups (p=0.8433732), while significant variations were observed among other groups (New Figure 3A).

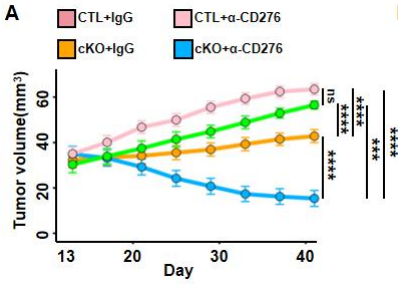

New Figure 3A.The tumor growth curves of different groups of mice were plotted. Measurements were taken every 4 days. P values were calculated by one-way ANOVA and Tukey HSD test.

3.In Figure 2F, comparing cKO+IgG group and cKO+a-CD276 group, although both group showed increased CD8^{+} cells, only cKO+a-CD276 group showed dramatic increase of Gzmb^{+}Cd8^{+}/Cd8^{+} ratio. This result indicates that CD8^{+} cell activation is crucial in anti-CD276 therapy. This observation needs further investigation.

Response: Thank you for your constructive comments. In our study, we concentrated on evaluating control, resistant, and sensitive mouse groups depicted in Figure 1 at three distinct time points. Considering the hypothesis that analyzing staining 41 days post-treatment might better represent the status of residual disease rather than initial anti-tumor mechanisms, we adhered to the established protocols for mouse tumor induction and treatment. Consequently, we collected samples from six mice in each group for additional staining analysis 13 and 27 days following α-CD276 treatment. Our findings reveal a notable upregulation of both $CD8^+$ T cells and $GZMB^+CD8^+$ T cells in the sensitive group (New Figure S1D and E), corroborating the notion that CD276 can dampen T cell activation and proliferation, facilitate tumor immune escape, and modulate immune responses and tumor dynamics via various signaling pathways, thus mitigating the suppression of tumor-infiltrating T cells upon CD276 inhibition (PMID: 36284349, 36869048, 37163614). Despite these insights, the exact ligands for CD276 remain unidentified, and the specific molecular processes through which CD276 suppresses $CD8^+$ T cell functionality are still under investigation. To address this gap, we have conducted protein arrays for the high-throughput identification of potential CD276 protein ligands; however, the definitive ligands and their regulatory mechanisms warrant further exploration.

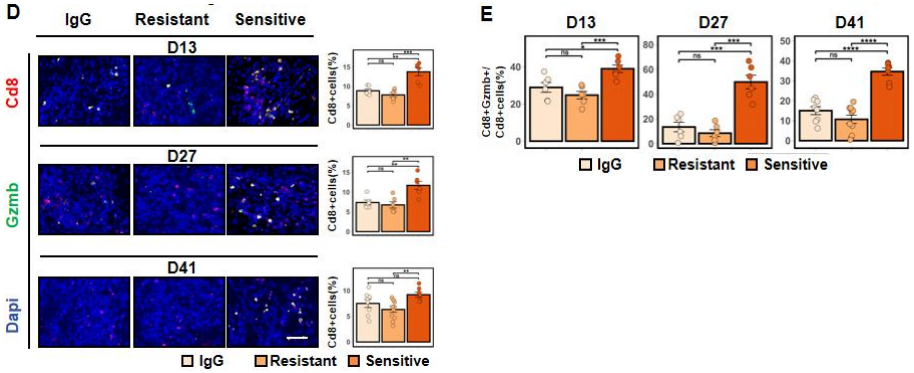

New Figure S1D and E. Representative immunofluorescence (IF) staining images of CD8 (green) and GZMB (red) (D). Statistical analysis of the ratio of $CD8^+$ cells and $CD8^+$ $GZMB^+$ cells to $CD8^+$ cells (CD8T killing capacity) (E) in different treatment groups . Scale bar, 25μm. Data are expressed as mean ± SD (Day 41 IgG=8, Resistant=11, Sensitive=7, Day 13 and 27 n=6). P values are presented by one-way ANOVA with Tukey's multiple comparison test.

4.The authors need to show if depleting PF4-positive cells will impact the sensitivity of the cells to a-CD276.

Response: We appreciate your constructive comments and have implemented the suggested revisions in the revised manuscript. Indeed, we had previously recognized the issue mentioned and bred Pf4Cre;DTR mice, which allow us to ablate PF4+ lineage cells upon diphtheria toxin treatment. However, the problem of this mouse model is that we can not exclude the early lineage of PF4 expressing cell, which at the time of toxin treatment could be PF4 negative but still can be depleted. Recognizing

this problem, we have ordered a custom Pf4CreERT mouse strain and successfully bred a more stringent Pf4creERT; RosaDTA mouse model. However, challenges associated with the timing of the induction phase prevented our initial manuscript from showcasing pertinent data promptly. Updated results illustrate that tamoxifen treatment markedly reduces PF4+ macrophage levels and augments the response of 4NQO-induced HNSCC mice which are resistant to α-CD276 therapy. New Figure 5E illustrates our strategic approach. Comparative analysis of lesion number, area, and histopathology indicates that, compared to the control group treated with IgG (Pf4-ctl), the combined treatment with Pf4-ctl and α-CD276 does not significantly inhibit tumor progression (New Figure 5F-I). Conversely, the Pf4-cKO group treated with IgG showed a moderate decrease in tumor growth, a trend that was more pronounced in the Pf4-cKO group treated with α-CD276 (Figures 5F-I).

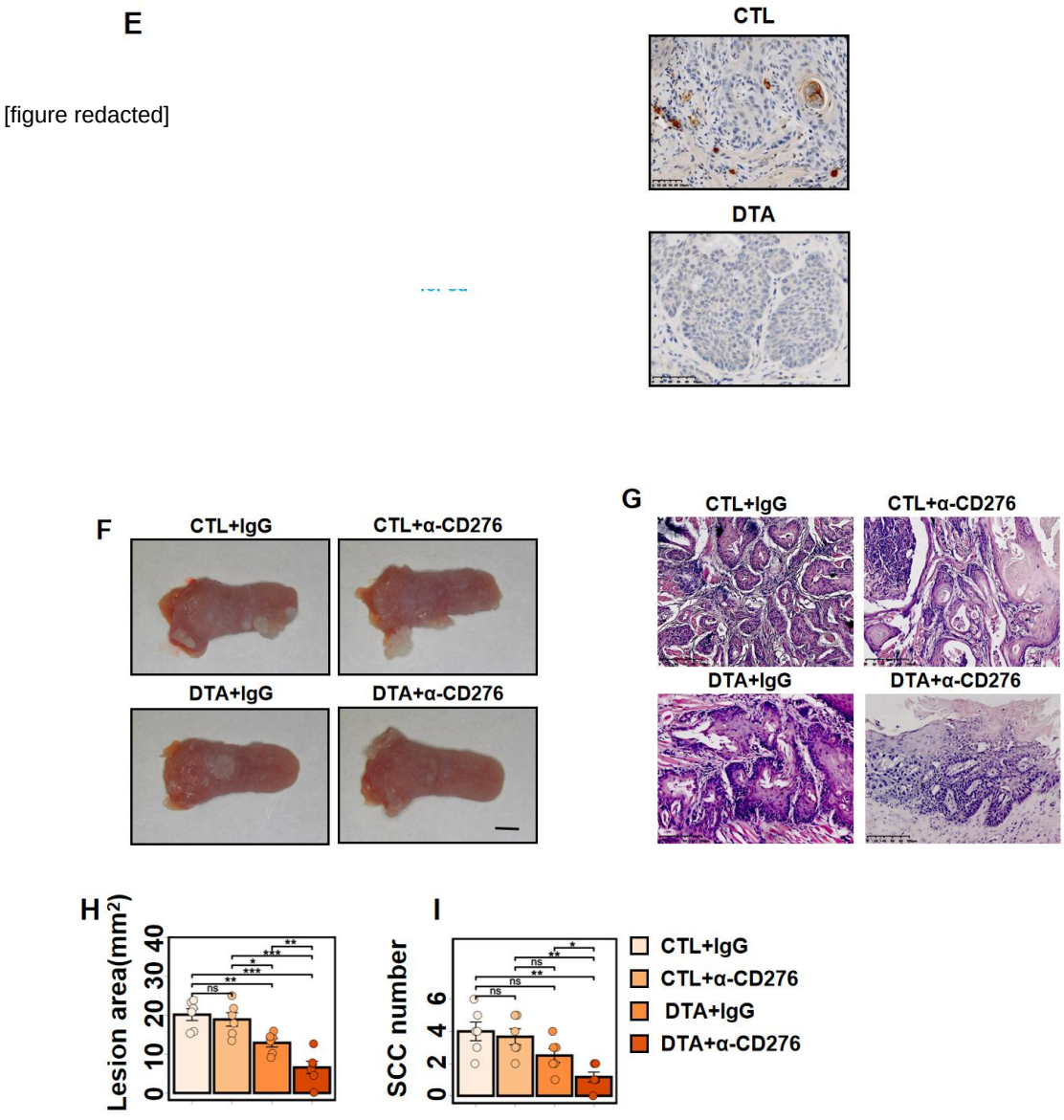

New Figure 5E-I. E. The experimental design of the HNSCC tumorigenesis model and treatment strategy (left) and representative image of PF4 IHC staining in CTL

(upper) and DTA (down) groups (right). F. Representative image of 4NQO-induced HNSCC in different groups. Scale bar, 1mm (right). G. Display of histological characteristics of HNSCC in different groups by H&E. Scale bar, 100μm. H and I. Quantification of tongue lesion area (H) and SCC number (I) in in different treatment groups. P values were calculated by one-way ANOVA with Tukey's multiple comparison test.

5.Does the ITGB6-CX3CL1 axis also recruit other suppressive cells, such as Treg cells, which may also be activated by STAT3?

Response: Thank you for your valuable suggestion. In response, we have enhanced our analysis by distinctly categorizing CD4 T cells into CD4 TH and Tregs within our single-cell datasets(New Figures 4F and S5B). This detailed analysis did not reveal significant changes in Treg populations between the CTL and the cKO group. Furthermore, we utilized flow cytometry to closely examine Treg dynamics during ITGB6 gene elimination (New Figures S4K and L) and following the combined ITGB6 knockout and α-CD276 treatment (New Figure S5N and O). These experiments confirmed that the absence of ITGB6 does not markedly affect Treg infiltration. Enclosed are the relevant images from our manuscript that illustrate these results.

New Figure 4F and S5B

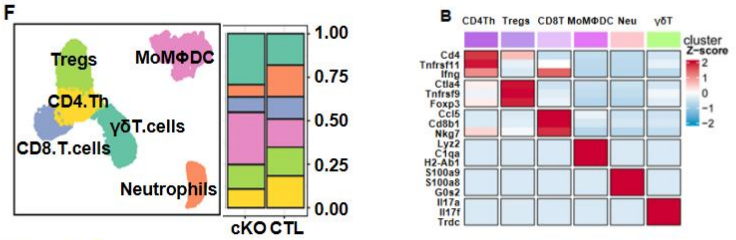

New Figure S4K and L

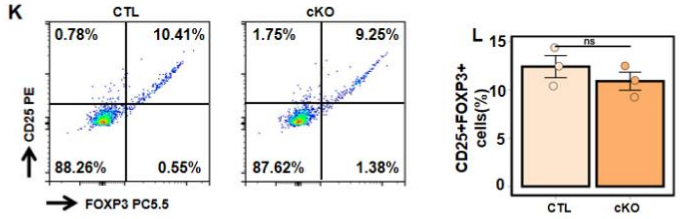

New Figure S5N and O

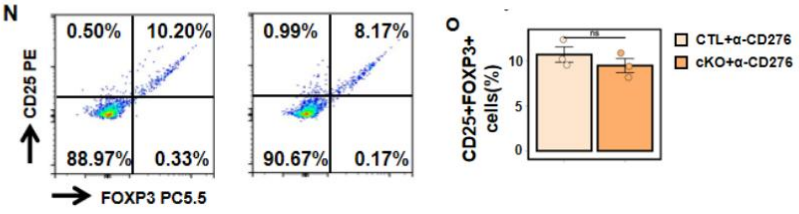

New Figure 4F. The UMAP diagram of the immune cell subpopulation (left) and the cell ratio between the two groups (right).

New Figure S5B. Heatmap of signature genes for Immune cells subclusters from mouse HNSCC tumor tissues. Each cell cluster is represented by three specifically expressed genes.
New Figure S4K and L . Representative flow plots show frequency of Tregs (K) and quantification of the proportions of Tregs (L) in CTL and cKO mice. P values were calculated by two-tailed unpaired Student's t-test.
New Figure S5N and O. Representative flow plots show frequency of Tregs (N) and quantification of the proportions of Tregs (O) in different treatment groups. P values were calculated by two-tailed unpaired Student's t-test.

6.The results of Fig. S2D-F should be shown as the main figures in the article, since these are the key findings of this project.

Response: Thank you for your valuable input on the importance of the results depicted in Fig. S2D-F. Heeding your advice, we have decided to transfer these results to the main figures section of our manuscript (New Figure 2A-C). We concur that these findings are integral to the core conclusions of our research and warrant greater visibility. This modification will highlight these crucial findings to readers more directly and emphasize their significance within the overarching narrative of our study.

7.Address issues of poor writing and editing, ensuring proper labeling of figures and supplementary figures for clarity. The figure # and supplementary figure# are not labeled which makes the manuscript very difficult to read.

Response: Thank you for highlighting the clarity and figure labeling issues within our manuscript. We recognize the critical importance of clear communication and are committed to extensively revising the document to enhance its readability and coherence. We will take special care to ensure that all figures and supplementary figures are accurately labeled and correctly referenced within the text, thereby improving the manuscript's overall readability and facilitating a better understanding of our research findings among readers.

Minor concerns,
1. The abstract: "Enoblituzumab is an immunotherapeutic agent targeted at CD276, demonstrating both safety and efficacy in the activation of T cells and oligodendrocyte-like cells against a variety of cancers. Nonetheless, numerous patients have not realized clinical benefits, and the mechanisms underlying resistance to α-CD276 therapy remain inadequately understood." Enoblituzumab has not been approved by the FDA for patient treatment yet. Thus, this statement is not applicable.

Response: Thank you for your suggestion; we have implemented the recommended changes. The updated description states, 'Mouse models and preclinical studies suggest that therapies targeting CD276 may be more effective compared to those

aimed at PD1 and PD-L1. Nevertheless, the data from the mouse model indicate a substantial non-responsive population to α-CD276 treatment, with the mechanisms underlying this resistance yet to be fully elucidated. '

2.The introduction should be more comprehensive and reader friendly, providing context on the significance of $PF4^+$ Macrophages and $GZMB^+$ T cells.

Response: Thank you for your feedback. We have updated the introduction to more effectively elucidate the significance and functions of $PF4^+$ macrophages and $GZMB^+$ T cells, both within the scope of our research and the wider scientific community. Our goal is to render the introduction more comprehensible and informative, thus offering readers a more transparent insight into the research backdrop and the distinct scientific inquiries we are exploring.

3. Fig. 1, the labels in Fig. 1F and 1K, “stress” or “sress”?

Response: Thank you for your reminder. We have made the necessary revisions accordingly.

4. Fig. 2C: The ITGB6 KO tongue tissue seems to bear more tumor. How do you quantify the tumor size and mass?

Response: Thank you for emphasizing this important point. In our research, the measurement of tumor size and mass within tongue tissues utilized two primary approaches: in vivo assessments were performed with digital calipers using a conventional formula to determine tumor volume; post-mortem, tumors were enumerated, and histological evaluations were conducted to analyze tumor area. Furthermore, for improved clarity and reader comprehension, we have delineated the tumor burden areas within the tongue tissue images.

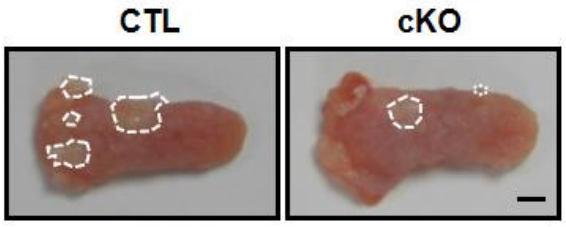

5. Fig. 4E: The text mentions that ITGB6 KO downregulates CX3CL1 mRNA transcription, by what experiment?

Response: Thank you for your inquiry. In our study, we compared the mRNA expression levels of CX3CL1 utilizing single-cell data from the CTL and cKO mouse groups, as depicted in Figure 4.

6.Fig. S4F: The text mentions that this figure shows a CX3CL1 decrease when

knockout ITGB6 in IHC, but the data is somehow vague, do you have a western blotting result?

Response:Thank you for your suggestion. We have incorporated the Western blot results for CX3CL1 into our manuscrip (New Figure S5G).

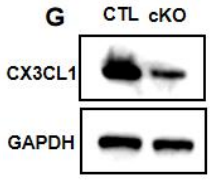

New Figure S5G. Western blotting analysis of CX3CL1 in control and cKO mice.

7.Fig. S4I: Lack of labeling, STAT3 IP/ IgG IP?

Thank you for your reminder. We have made the necessary revisions accordingly.

8. The title needs to be more specific to CD276 targeting immunotherapy.

Thank you for your suggestion. In the revised manuscript, we have investigated the role of ITGB6 in the resistance mechanism to α- PD1 treatment. To explore the role of ITGB6 in mediating resistance to α-PD1 therapy, we employed a comparable approach and administered α-PD1 or IgG to 4NQO-induced carcinogenic mice for 13 days. The α-PD1 was delivered intraperitoneally at a dose of 10 mg/kg every four days, consistent with previous protocols, amounting to four total doses (Fig. 9A). Tumor progression was monitored bi-weekly from the initial α-PD1 administration via MRI (Fig. 9B). Resistance was characterized by an early response in MRI imaging followed by an increase to more than 120% of the initial size, according to RECIST criteria (Fig. 9B). Thirteen days after the first injection, tongues of the HNSCC-bearing mice were removed (Fig. 9C), revealing reduced malignancy, invasion area, and tumor count in the αPD1-sensitive group compared to the control and resistant groups (Fig. 9C). IHC analysis showed a marked decrease in ITGB6 expression in the sensitive group (Fig. 9D). Furthermore, increased infiltration of $PF4^{+}$ macrophages was observed in the resistant group (Fig. 9E). To determine ITGB6's contribution to α-PD1 treatment efficacy, 12 αPD1-resistant mice were divided into two groups: one continued with the PD1 antibody while the other was treated with a combination of PD1 and the ITGB6 antibody 264RAD. This method notably restored α-PD1 treatment responsiveness in the mice (Fig. 9F and G). The overall analysis of lesion quantity and area demonstrated that ITGB6 inhibition reinstates α-PD-1 treatment sensitivity in mice (Fig. 9H and I). Below, we provide detailed descriptions and images incorporated into the manuscript to highlight these results (New Figure 9). As indicated in our a-PD1 treatment data, ITGB6 appears to be a common mechanism in resistance to immune checkpoint inhibitor. Hence, blocking ITGB6 would likely be beneficial in either single agent or combination therapy scenario.

[figure redacted]

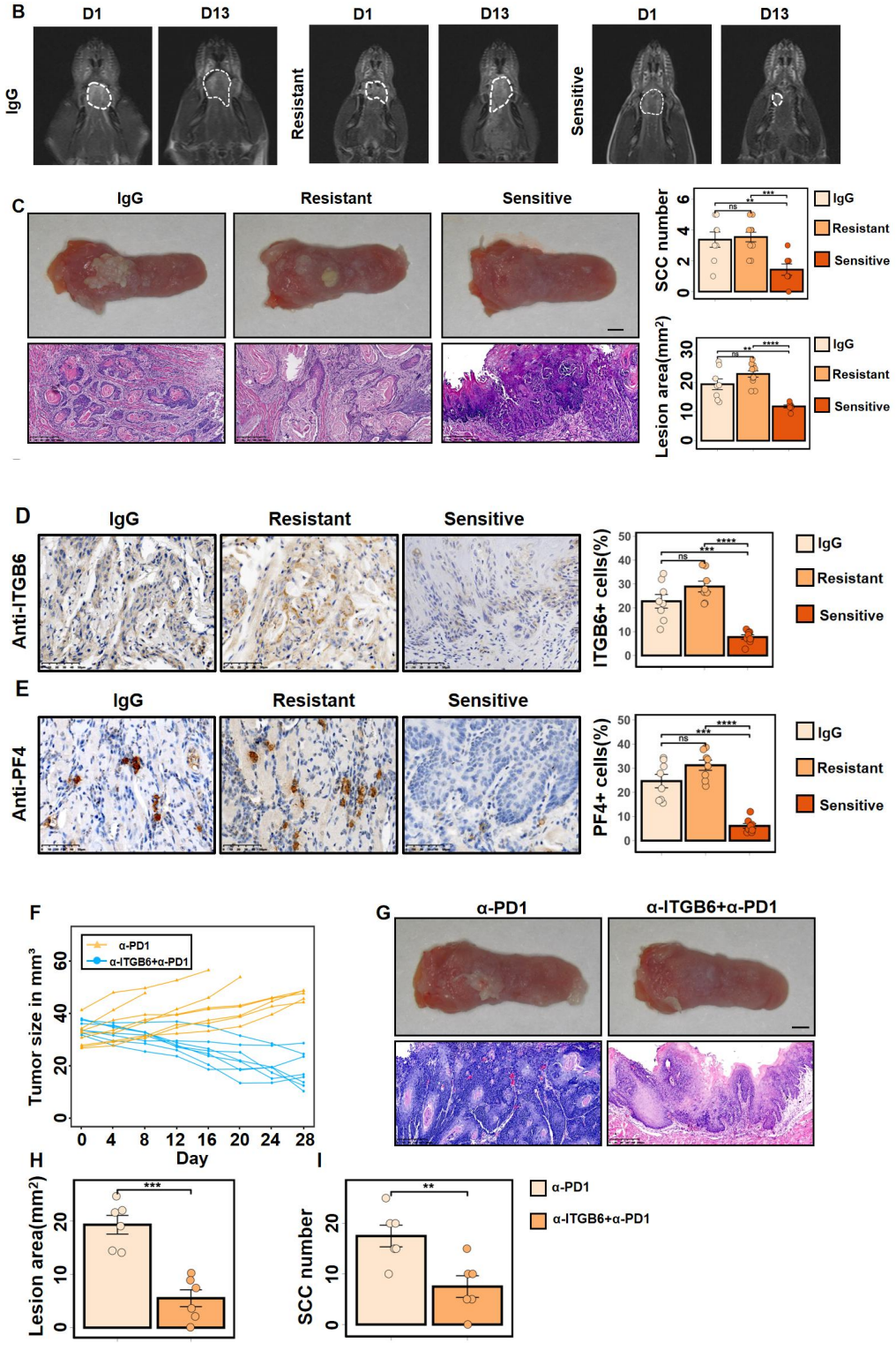

New Figure 9. A.The experimental design of the HNSCC tumorigenesis model and

treatment strategy. B. Representative examples of head and neck magnetic resonance imaging (MRI) for different groups. The dashed area is the boundary of the tumor. C. Representative images of 4NQO induced HNSCC (upper) and corresponding HE staining (lower) (left). Quantification of SCC number (upper) and tongue lesion area (lower) (right) in different treatment groups. Scale bar, 1mm (upper), 100μm (lower). P values are presented by one-way ANOVA with Tukey's multiple comparison test. D and E. Representative images of ITGB6 (D), PF4 (E) IHC staining (left) and quantification of percentage of $ITGB6^{+}$ (D), $PF4^{+}$ (E) (right) in different treatment groups. Scale bar, 50μm. Data are presented as mean ± SD (n=8). P values are presented by one-way ANOVA with Tukey's multiple comparison test. F.Tumor growth curves for each mouse treated with either the combination of α-PD1 and α-ITGB6 or the control α-PD1 treatment, with measurements recorded every four days. G.Representative images of 4NQO induced HNSCC (upper) and corresponding HE staining(lower). Scale bar, 1mm (upper), 100μm (lower). H and I.Quantification of tongue lesion area (H) and SCC number (I) in different groups. P values were calculated by two-tailed unpaired Student's t-test.

REVIEWER COMMENTS

Reviewer #2 (Remarks to the Author):

The authors have answer most of my comments. However, since all monocyte-derived TAMs are decreased in ITGB6ko mice or mice treated with anti-CX3CR1 antibody, it is not clear whether PF4+ macrophages are the sole population leading to resistance to treatment. The data pointing toward a role of PF4+ macrophages are only based on CellChat, gene enrichment pathways and human correlative studies. The co-culture assay does not compare PF4+ macrophages to other monocyte-derived TAM subsets.

To prove that PF4+ macrophages are specifically involved in this setting, authors should complement an ITGB6ko mice with WT PF4+ macrophages.

Reviewer #3 (Remarks to the Author):

The authors did not addressed adequately the issues that were raised notably on the nature of the cells as well as the mechanistic aspects.

Also flow cytometry data presented (for example New Figure S4K-L) is not presented at publication standards with clear compensation issue.

Reviewer #4 (Remarks to the Author):

The authors have made some improvements to the manuscript, addressing most of my previous concerns. However, there are still several issues that need to be addressed before considering the manuscript for acceptance. My primary issue is with the overall quality of the writing. The manuscript suffers from unclear logic, ambiguous descriptions of experiments, verbosity, and numerous instances of mislabeling and typographical errors.

Areas for Improvement:

The narrative structure of the manuscript could be enhanced by reorganizing the content to ensure a more logical flow of information. Including a schematic diagram to illustrate the overall research design would greatly aid in understanding.

The effect of ITGB6 in inhibiting T cells has been well documented in previous studies (as

another reviewer pointed out). The current study's identification of a new pathway involving ITGB6 and T cell exhaustion is noteworthy. It would be beneficial to discuss relevant previous studies, such as the one with PMID: 35131862, in the introduction and highlight what are the unknown aspects before this manuscript.
There is an inconsistency in Figure 3A between the colors used for callout labels and the corresponding curves in the graph.
The mechanism by which PF4+ macrophages regulate CXCR6+CD8+ T cells remains unclear and requires a clearer explanation.

Reviewer #5 (Remarks to the Author):
The authors have shown a willingness to address the comments and provided ample new data. This is appreciated and beneficial for the manuscript. Yet, some remarks remain.

1. Since all of the work except figure 9 is on aCD276 therapy, this should be part of the title. The data in figure 9 confirming the resistance mechanism also for aPD1 therapy is of added value. Given aCD276 is trialled together with aPD1 for HNC, this combination would have increased clinical utility.

2. Tumor response is evaluated via tumor grade, lesion area and SCC number. The choice for these parameters over conventional complete responses should be explained. The methodology of assessing these parameters should be clearly described. Visual aid in the first H&E images to support the reader in visually understanding the parameters is warranted. Why are MRI or digital caliper measurements not used consistently?

3. Given the goal of tumor elimination, it is imperative to delineate Caspase-3 staining on tumor cells over stromal cells. This should be assessed. Current image quality does not allow the readers to thoroughly and unequivocally assess it themselves.

We sincerely appreciate the invaluable comments and insights provided by the reviewers. We have thoroughly considered their critiques and suggestions, and have made diligent efforts to address all concerns raised. Significant new data have been added to both the main and supplementary figures, directly responding to the issues highlighted in the initial review. As a result, our manuscript has been substantially improved, offering a stronger and clearer presentation of our findings. We are grateful for the reviewers' guidance, which has considerably enhanced our research. Furthermore, we thank the reviewers for their patience during the extended revision process, necessitated by the comprehensive experimental work required. Their understanding and willingness to evaluate the revised manuscript are highly appreciated.

Reviewer #1
Reviewer #2 (Remarks to the Author):

The authors have answer most of my comments. However, since all monocyte-derived TAMs are decreased in ITGB6ko mice or mice treated with anti-CX3CR1 antibody, it is not clear whether PF4+ macrophages are the sole population leading to resistance to treatment. The data pointing toward a role of PF4+ macrophages are only based on CellChat, gene enrichment pathways and human correlative studies. The co-culture assay does not compare PF4+ macrophages to other monocyte-derived TAM subsets.
To prove that PF4+ macrophages are specifically involved in this setting, authors should complement an ITGB6ko mice with WT PF4+ macrophages.

Response: Thank you for your insightful feedback. We have conducted additional experiments and incorporated the relevant findings into the revised manuscript to address your concerns. Indeed, we had previously recognized the issue mentioned and bred Pf4Cre;DTR mice, which allow us to ablate PF4+ lineage cells upon diphtheria toxin treatment. However, the problem of this mouse model is that we can not exclude the early lineage of PF4 expressing cell, which at the time of toxin treatment could be PF4 negative but still can be depleted. Recognizing this problem, we have ordered a custom Pf4CreERT mouse strain and successfully bred a more stringent Pf4creERT; RosaDTA mouse model. However, challenges associated with the timing of the induction phase prevented our initial manuscript from showcasing pertinent data promptly. Updated results illustrate that tamoxifen treatment markedly reduces PF4+ macrophage levels and augments the response of 4NQO-induced HNSCC mice which are resistant to α-CD276 therapy. New Figure 5E illustrates our strategic approach. Comparative analysis of lesion number, area, and histopathology indicates that, compared to the control group treated with IgG (Pf4-ctl), the combined treatment with Pf4-ctl and α-CD276 does not significantly inhibit tumor progression (New Figure 5F-I). Conversely, the Pf4-cKO group treated with IgG showed a moderate decrease in tumor growth, a trend that was more pronounced in the Pf4-cKO group treated with α-CD276 (Figures 5F-I).

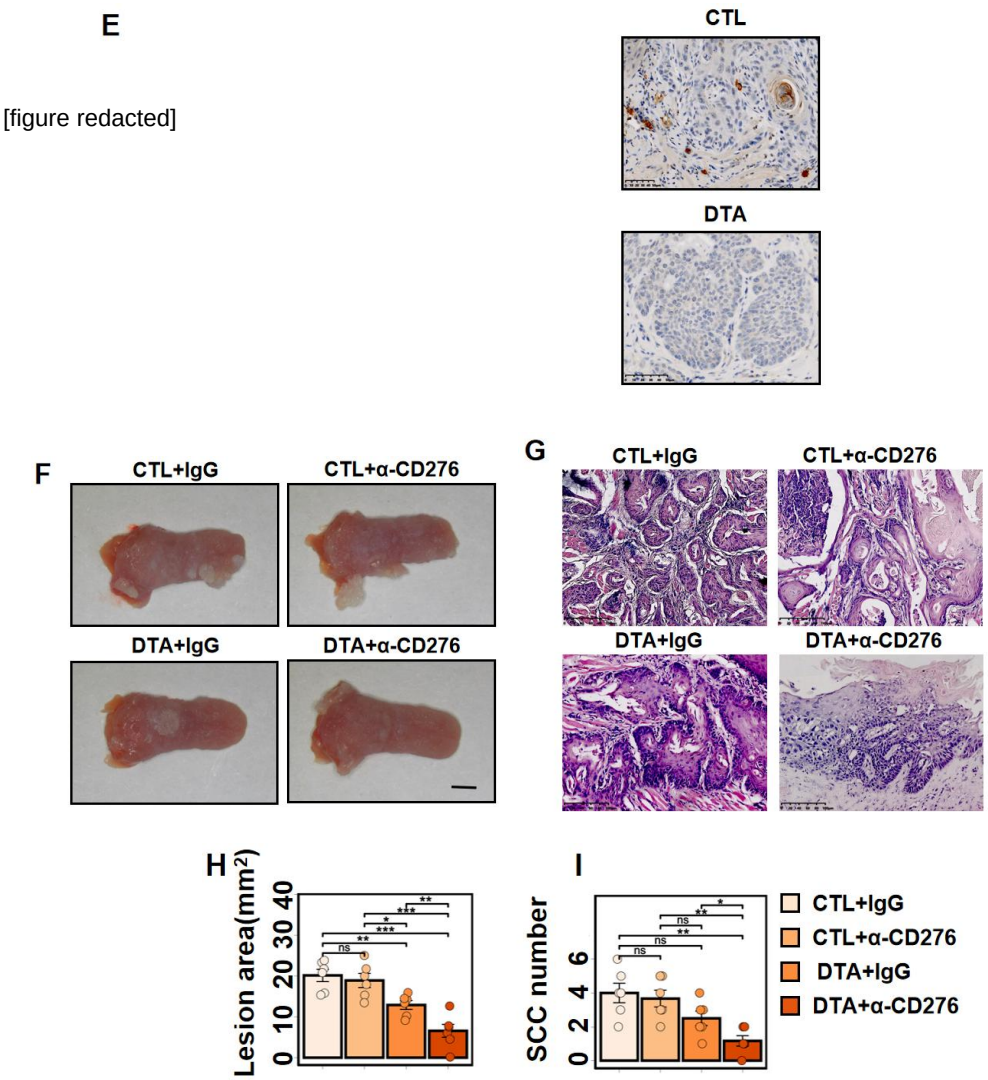

New Figure 5E-I. E. The experimental design of the HNSCC tumorigenesis model and treatment strategy (left) and representative image of PF4 IHC staining in CTL (upper) and DTA (down) groups (right). F. Representative image of 4NQO-induced HNSCC in different groups. Scale bar, 1mm (right). G. Display of histological characteristics of HNSCC in different groups by H&E. Scale bar, 100μm. H and I. Quantification of tongue lesion area (H) and SCC number (I) in in different treatment groups. P values were calculated by one-way ANOVA with Tukey's multiple comparison test.

Reviewer #3 (Remarks to the Author):
The authors did not addressed adequately the issues that were raised notably on the nature of the cells as well as the mechanistic aspects.
Also flow cytometry data presented (for example New Figure S4K-L) is not presented at publication standards with clear compensation issue.

Response: Thank you for your constructive feedback and suggestions, and for giving us the opportunity to address your concerns and enhance the quality of our manuscript. Upon identifying ITGB6 as a key gene mediating resistance to CD276 antibody

therapy, we initially assessed its direct impact on tumor growth and invasion. Our previous results demonstrated that ITGB6 does not significantly affect tumor growth or invasion. Subsequent analyses confirmed that ITGB6 promotes the infiltration of PF4+ macrophages into the tumor microenvironment. From a mechanistic perspective , knockout of ITGB6 greatly reduced the mRNA expression of CX3CL1 in tumor cells (Fig. S6E). In addition, IHC staining of CX3CL1 similarly showed that knockdown of Itgb6 significantly downregulated CX3CL1 protein expression (Fig. S6F). Furthermore, our western blot experiments confirmed that the knockout of ITGB6 results in the downregulation of the expression level of CX3CL1 (Fig. S6G). To probe the possible mechanism of how ITGB6 mediates CX3CL1 expression, we first performed SCENIC analysis and found 21 downregulated inferred transcription factors (Fig. S6H, Table S3). In addition, we used tools from online UCSC Genome Bioinformatics Site (http://genome.ucsc.edu/) and found 25 predicted transcription factors at the promoter of Cx3cl1 gene (score>10 and relative score>0.95) (Table S4). Of note, Stat3 was the common transcription factor between SCENIC analysis and online analysis (Fig. S6I). Subsequently, to investigate whether STAT3 can bind to the promoter of Cx3cl1 gene, we used Moc1 cells and performed chromatin Immunoprecipitation quantitative real-time PCR (ChIP-qPCR) assay using antibodies against STAT3 or IgG (control). We observed enriched occupancy of STAT3 at the promoter regions of CX3CL1 gene compared to the IgG control, whereas STAT3 knockdown significantly reduced the binding of STAT3 to the promoter of Cx3cl1 (Fig. S6J). To clarify how ITGB6 regulates STAT3, we further focused on all downstream signaling pathways related to the integrin family, including FAK/SRC, ERK1/2, NFKB1, SAPK/JNK, PI3K/AKT, and P38 MAPK (Cooper and Giancotti, 2019; Li et al., 2021; Liu et al., 2023; Slack et al., 2022). Among these pathways, we found that ITGB6 knockout can reduce the phosphorylation of FAK/SRC (Fig. S6K). Our scRNAseq data revealed that CX3CR1 is specifically expressed in PF4+ macrophages (Fig. S6L). To validate that, we conducted immunofluorescence (IF) staining and detected co-expression of CX3CR1 and PF4 (Fig. S6M). Through both patient-derived and murine models, we observed a significant correlation between the presence of PF4+ macrophages and poorer patient survival, as well as their role in promoting the exhaustion of tumor-specific CXCR6+ CD8+ T cells.

To delve deeper into the mechanisms by which PF4+ macrophages induce exhaustion of CXCR6+ CD8+ T cells, we performed differential gene expression analysis. The results revealed that the GZMB+ CXCR6+ CD8+ T cell subset was predominantly enriched in immune response and antigen processing pathways, indicative of immune activation. In contrast, the PDCD1+ CXCR6+ CD8+ T cell subset was enriched in lectin C and glycolysis pathways, suggestive of an exhausted state (Figures S12A and S12B). SCENIC analysis of our single-cell data further revealed elevated CREM gene expression in the PDCD1+ CXCR6+ CD8+ T cell group (Figure S12C). To substantiate the role of CREM in CD8+ T cell exhaustion, we analyzed CD8+ T cell data from Robert L. Ferris et al., confirming high CREM activity in the PDCD1+ CXCR6+ CD8+ T cell subset (Figure S12D).

We also explored the regulation of CREM activity by the CXCL16-CXCR6 axis

by isolating CD8+ T cells from tumor tissues and stimulating them with recombinant CXCL16 protein at concentrations of 100 ng/ml and 800 ng/ml (Figure S12E). Our findings indicated that the lower CXCL16 concentration resulted in a significant decrease in PDCD1+ CXCR6+ CD8+ T cells and an increase in GZMB+ CXCR6+ CD8+ T cells compared to the higher concentration group (Figures S12F and S12G). Western blot analysis of sorted PDCD1+ CXCR6+ CD8+ T cells and GZMB+ CXCR6+ CD8+ T cells demonstrated a notable increase in CREM levels in the GZMB+ CXCR6+ CD8+ T cell subset, suggesting that CREM may mediate the exhaustion process in CXCR6+ CD8+ T cells (Figure S12H).

In cancer, CREM contributes to tumor immune evasion by fostering an immunosuppressive microenvironment. Targeting CREM pathways may enhance the effectiveness of cancer immunotherapies by preventing tumor-induced immune suppression (PMID: 17097831). Notably, a recent study published in Cell has also highlighted the close association between CREM and the function of CD8+ T cells (PMID: 38744281). Consequently, our findings highlight the potential of targeting CREM to restore the functionality of exhausted CXCR6+CD8+T cells.

Similarly, we have included the graphic abstract of the overall design below for your convenience and to facilitate your review (Graphic Abstract).

Additionally, we have resolved the compensation issues in our flow cytometry data and enhanced the quality of the figures to meet publication standards. The revised figures now clearly and accurately reflect our findings.

New Figure S6E-N

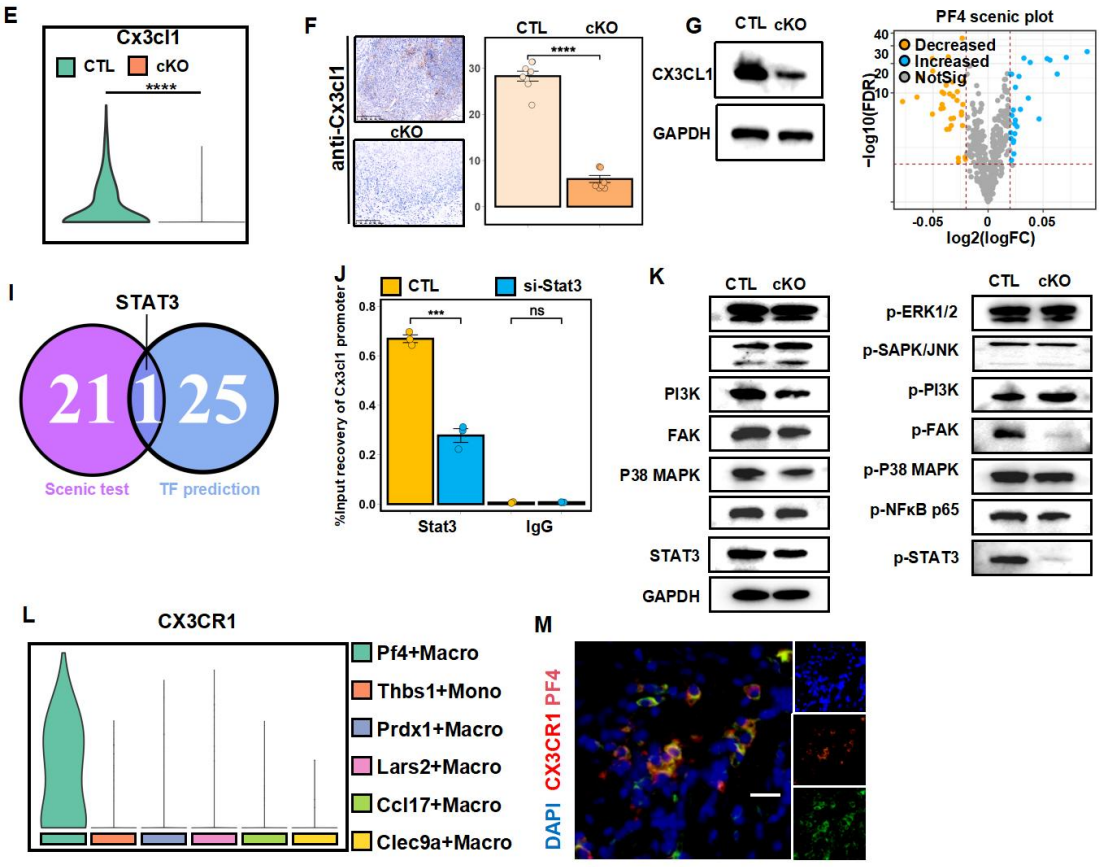

New Figure S12

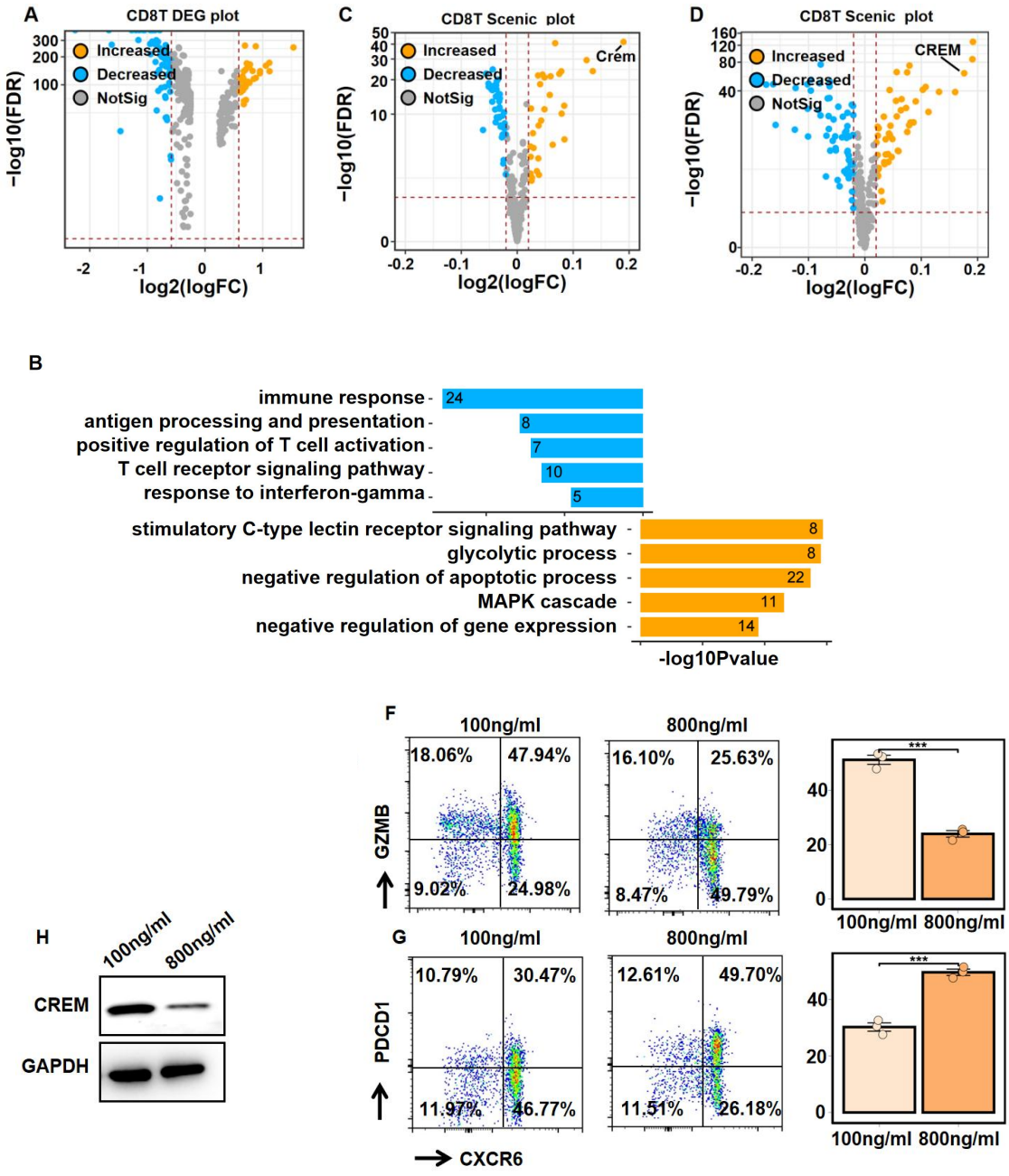

New Figure S6E-N E.Violin plot showing the expression of CX3CL1 in epithelial cells between the two groups. F.Representative images of CX3CL1 IHC staining (left) and quantitation of the percentage of CX3CL1+ cells (right) in different treatment groups. Scale bar, 50μm. Data are shown as mean ± SD (n = 8). P values were calculated by two-tailed unpaired Student's t-test. G.Western blotting analysis of CX3CL1 in control and cKO mice. H.Volcano plot showing differences in transcription factors of tumor cells between the two groups, transcription factors derived from Scenic analysis. I.Venn diagram showing Stat3 as overlaped transcription factor between Scenic and online analysis. J. ChIP-qPCR analysis of Stat3 binding to CX3CL1. Data were presented as mean ± SD (n=3). P values were calculated by two-tailed unpaired Student's t-test. K. Western blotting analysis of

ERK1/2, SAPK/JNK, PI3K, AKT, FAK, P38 MAPK, NFKB1, STAT3 and analysis of phosphorylated ERK1/2, SAPK/JNK, PI3K, AKT, FAK, P38 MAPK, NFKB1, STAT3 in control and cKO Moc1 cells. L. Violin plot showing the expression of Cx3cr1 in all cell types. M. Immunofluorescence staining to detect expression of mice CX3CR1 (red), and PF4 (green) . DAPI was used for nuclear staining. Scale bar, 25 μm. N. Representative flow plots show frequency of Tregs (upper) and quantification of the proportions of Tregs (down) in different treatment groups. P values were calculated by two-tailed unpaired Student's t-test.

New Figure S12. A. Differential expression analysis identifies differences in $GZMB^+CXCR6^+CD8^+$T cells and $PDCD1^+CXCR6^+CD8^+$T cells. Differential expression analysis by DEseq2. Volcano plots demonstrating significant ($p<0.05$) differential ($|logFC|>0.585$) abundances. B. GO pathway enrichment analysis of differentially expressed genes of $CD8^+$T cells in different subsets. C. Volcano plot showing differences in transcription factors of $CD8^+$T cells between the two subsets, transcription factors derived from Scenic analysis. D. Volcano plot showing differences in transcription factors of $CD8^+$T cells between the two subsets in data from Robert L. Ferris et al, transcription factors derived from Scenic analysis. E. The experimental design of T cell killing experiments. F. Representative flow plots show frequency of the $CXCR6^+$ $CD8^+$ $GZMB^+$ T cells (left) and quantification of the proportions of $CXCR6^+$ $CD8^+$ $GZMB^+$ T cells (right) in groups different CXCL16 doses. P values were calculated by two-tailed unpaired Student's t-test. G. Representative flow plots show frequency of the $CXCR6^+$ $CD8^+$ $PDCD1^+$ T cells (left) and quantification of the proportions of $CXCR6^+$ $CD8^+$ $PDCD1^+$ T cells (right) in groups different CXCL16 doses. P values were calculated by two-tailed unpaired Student's t-test. H. Western blotting analysis of CREM in different subsets of $CXCR6^+CD8^+$T cells.

Graphic Abstract

[figure redacted]

New Figure S5K and L

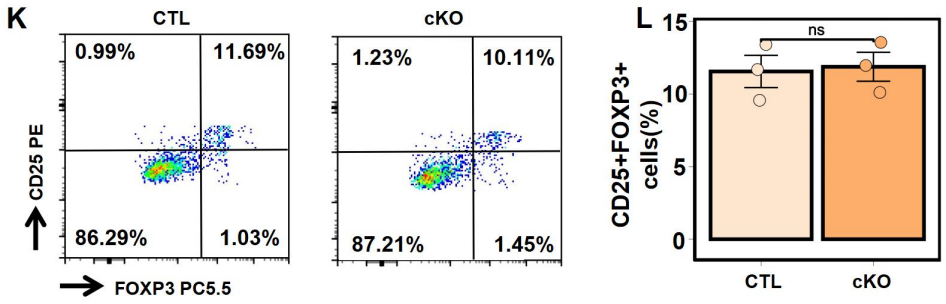

New Figure S6N

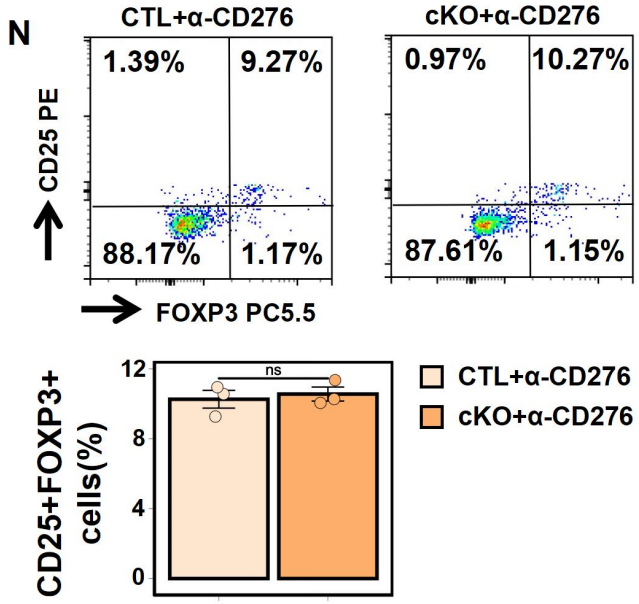

New Figure S5K and L . Representative flow plots show frequency of Tregs (K) and quantification of the proportions of Tregs (L) in CTL and cKO mice. P values were calculated by two-tailed unpaired Student's t-test.

New Figure S6N. Representative flow plots show frequency of Tregs (upper) and quantification of the proportions of Tregs (down) in different treatment groups. P values were calculated by two-tailed unpaired Student's t-test.

Reviewer #4 (Remarks to the Author):

The authors have made some improvements to the manuscript, addressing most of my previous concerns. However, there are still several issues that need to be addressed before considering the manuscript for acceptance. My primary issue is with the overall quality of the writing. The manuscript suffers from unclear logic, ambiguous descriptions of experiments, verbosity, and numerous instances of mislabeling and typographical errors.

Response: Thank you for your positive feedback on our revised manuscript and for

your constructive suggestions. We engaged a professional language editing service to refine and polish the manuscript's language. Additionally, we meticulously revised and reorganized the figures and tables to enhance their logical flow and readability. Futhermoere, we have provided more detailed explanations in the Methods section and expanded the descriptions of experimental procedures to ensure clarity and thoroughness.

Areas for Improvement:
The narrative structure of the manuscript could be enhanced by reorganizing the content to ensure a more logical flow of information. Including a schematic diagram to illustrate the overall research design would greatly aid in understanding.

Response: Thank you for your valuable suggestions and feedback. We have reorganized the figures to enhance logical coherence and readability. Additionally, as per your advice, we have revised the graphical abstract and included relevant experimental design flowcharts in each figure.

[figure redacted]

The effect of ITGB6 in inhibiting T cells has been well documented in previous studies (as another reviewer pointed out). The current study's identification of a new pathway involving ITGB6 and T cell exhaustion is noteworthy. It would be beneficial to discuss relevant previous studies, such as the one with PMID: 35131862, in the introduction and highlight what are the unknown aspects before this manuscript.

Response: Thank you for your valuable feedback. We appreciate your suggestions, and have now addressed them comprehensively. Although our initial manuscript did discuss the findings of the article with PMID: 35131862, we have now expanded our analysis to provide a more thorough discussion. We have examined the commonalities between the two studies in greater detail and highlighted the novel discoveries made in our research.

There is an inconsistency in Figure 3A between the colors used for callout labels and the corresponding curves in the graph.
The mechanism by which PF4+ macrophages regulate CXCR6+CD8+ T cells remains unclear and requires a clearer explanation.

Response: Thank you for your valuable suggestions. We have corrected the labeling errors in the figure captions. Regarding the mechanism by which PF4+ macrophages promote the exhaustion of CXCR6+ CD8+ T cells through the CXCL16-CXCR6 axis, we have included additional details in the manuscript. Furthermore, we have added a comprehensive and detailed analysis of this mechanism in the Discussion section. Below, you will find the relevant images from the manuscript.

To further assess the influence of the CXCR6 receptor on $CD8^+$ T cell functionality and state, a differential gene expression analysis was carried out. The results revealed that the $GZMB^+$ $CXCR6^+$ $CD8^+$ T cell subgroup was predominantly enriched in pathways associated with the immune response and antigen processing and presentation, indicative of immune activation. Conversely, the $PDCD1^+$ $CXCR6^+$ $CD8^+$ T cell group displayed greater enrichment in lectin C and glycolysis pathways (Fig. S12A and B). A subsequent SCENIC analysis showed that CREM gene expression was significantly elevated in the $PDCD1^+$ $CXCR6^+$ $CD8^+$ T cell group (Fig. S12C). To further determine CREM's role in $CD8^+$ T cell depletion, SCENIC analysis was applied to $CD8^+$ T cells data from Robert L. Ferris et al., confirming high CREM activity in the $PDCD1^+$ $CXCR6^+$ $CD8^+$ T cell subgroup (Fig. S12D). To explore the possibility that CREM activity in this group is regulated by the CXCL16-CXCR6 axis, $CD8^+$ T cells were isolated from tumor tissues and subjected to activation with 100ng/ml and 800ng/ml concentrations of CXCL16 recombinant protein (Fig. S12E). Findings indicated that the low CXCL16 concentration group showed a significant decrease in the $PDCD1^+$ $CXCR6^+$ $CD8^+$ T cell fraction and an increase in the $GZMB^+$ $CXCR6^+$ $CD8^+$ T cell fraction compared to the high concentration group (Fig. S12F and G). Western blot analyses on sorted $PDCD1^+$ $CXCR6^+$ $CD8^+$ T and $GZMB^+$ $CXCR6^+$ $CD8^+$ T cells demonstrated a notable increase in CREM levels within the $GZMB^+$ $CXCR6^+$ $CD8^+$ T cell subgroup, suggesting that CREM may mediate the exhaustion process in $CXCR6^+$ $CD8^+$ T cells (Fig. S12H).

In cancer, CREM contributes to tumor immune evasion by fostering an immunosuppressive microenvironment. Targeting CREM pathways may enhance the effectiveness of cancer immunotherapies by preventing tumor-induced immune suppression (PMID: 17097831). Notably, a recent study published in Cell has also

highlighted the close association between CREM and the function of CD8+ T cells (PMID: 38744281). Consequently, our findings highlight the potential of targeting CREM to restore the functionality of exhausted CXCR6+CD8+T cells.

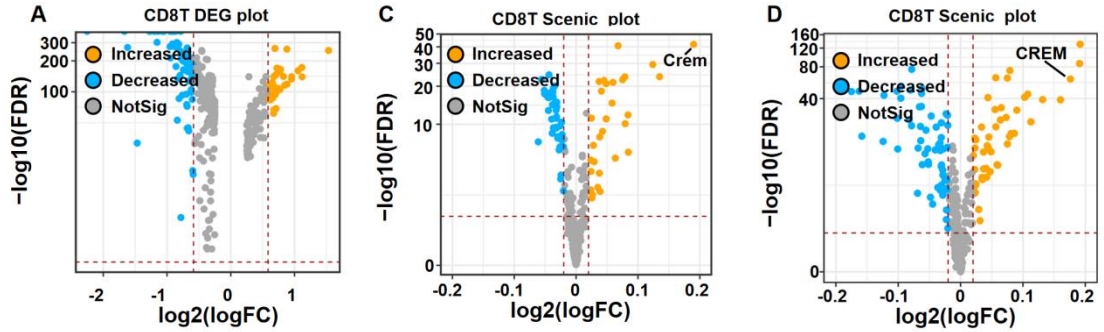

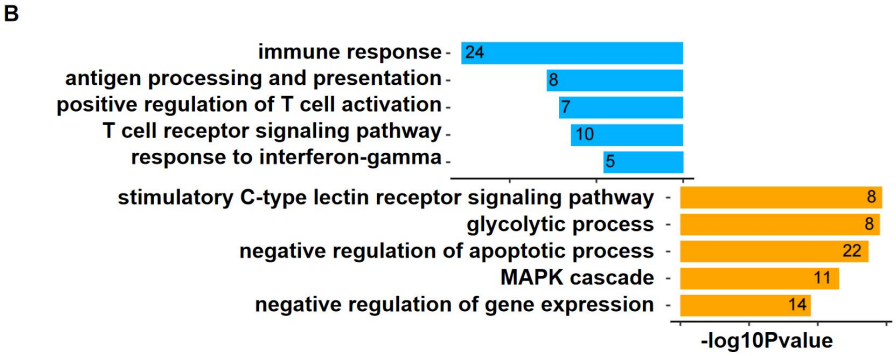

[figure redacted]

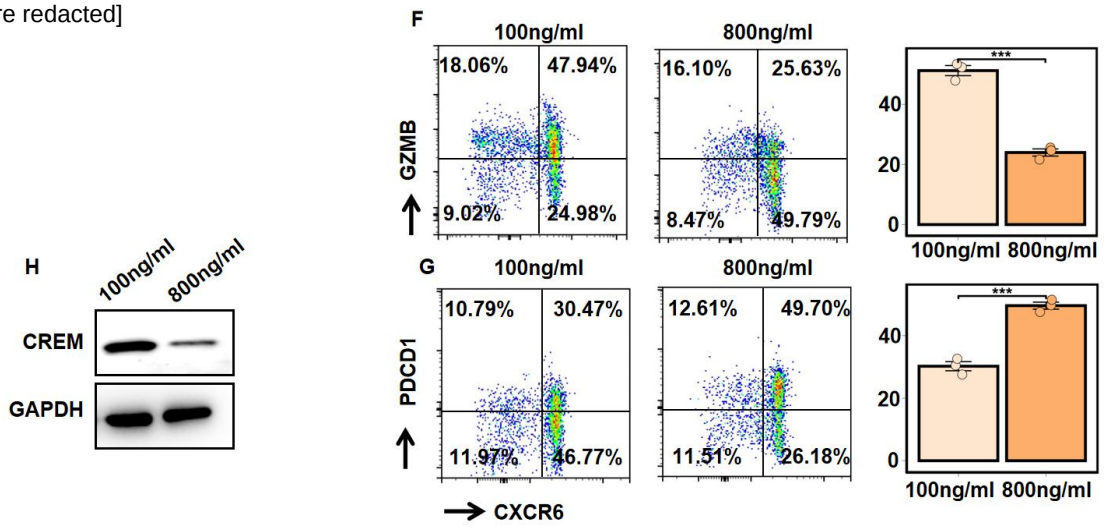

New Figure S12. A. Differential expression analysis identifies differences in GZMB^{+}CXCR6^{+}CD8^{+}T cells and PDCD1^{+}CXCR6^{+}CD8^{+}T cells. Differential expression analysis by DEseq2. Volcano plots demonstrating significant ($p<0.05$) differential ($|logFC|>0.585$) abundances. B. GO pathway enrichment analysis of differentially expressed genes of CD8^{+}T cells in different subsets. C. Volcano plot showing differences in transcription factors of

CD8$^+$T cells between the two subsets, transcription factors derived from Scenic analysis. D. Volcano plot showing differences in transcription factors of CD8$^+$T cells between the two subsets in data from Robert L. Ferris et al, transcription factors derived from Scenic analysis. E. The experimental design of T cell killing experiments. F. Representative flow plots show frequency of the CXCR6$^+$ CD8$^+$ GZMB$^+$ T cells (left) and quantification of the proportions of CXCR6$^+$ CD8$^+$ GZMB$^+$ T cells (right) in groups different CXCL16 doses. P values were calculated by two-tailed unpaired Student's t-test. G. Representative flow plots show frequency of the CXCR6$^+$ CD8$^+$ PDCD1$^+$ T cells (left) and quantification of the proportions of CXCR6$^+$ CD8$^+$ PDCD1$^+$ T cells (right) in groups different CXCL16 doses. P values were calculated by two-tailed unpaired Student's t-test. H. Western blotting analysis of CREM in different subsets of CXCR6$^+$CD8$^+$T cells.

Reviewer #5 (Remarks to the Author):
The authors have shown a willingness to address the comments and provided ample new data. This is appreciated and beneficial for the manuscript. Yet, some remarks remain.

Response: Thank you for your constructive feedback. Based on your suggestions, we have systematically addressed each point to enhance the quality of our manuscript. We appreciate your detailed review and are confident that these revisions have significantly strengthened the manuscript.

1. Since all of the work except figure 9 is on aCD276 therapy, this should be part of the title. The data in figure 9 confirming the resistance mechanism also for aPD1 therapy is of added value. Given aCD276 is trialled together with aPD1 for HNC, this combination would have increased clinical utility.

Response: Thank you for your valuable suggestions. In accordance with your feedback, we have incorporated information related to aCD276 into the manuscript title. As indicated in our a-PD1 treatment data, ITGB6 appears to be a common mechanism in resistance to immune checkpoint inhibitor. Hence, blocking ITGB6 would likely be beneficial in either single agent or combination therapy scenario.

2. Tumor response is evaluated via tumor grade, lesion area and SCC number. The choice for these parameters over conventional complete responses should be explained. The methodology of assessing these parameters should be clearly described. Visual aid in the first H&E images to support the reader in visually understanding the parameters is warranted. Why are MRI or digital caliper measurements not used consistently?
Response: Thank you for your insightful comments. Regarding the use of tumor grade, lesion area, and SCC number for evaluating tumor response, we selected these parameters based on their application in previous studies (PMID: 33945793, 28285905, 32697949), which have demonstrated their relevance and reliability in

mouse tumor models. We have included a detailed explanation of these choices in the methodology section and added visual aids in the form of annotated H&E images from our previous study to help readers understand how these parameters were assessed (PMID: 28285905). We also assessed tumor volume changes and clinical outcomes before and after treatment as you suggested, and the results were consistent with those obtained from tumor grade, lesion area, and SCC number. Initially, we utilized MRI for tumor assessment; however, due to COVID-19 pandemic restrictions, we were unable to continue MRI assessments and instead used digital caliper measurements. Comparative analysis between MRI and digital caliper measurements showed consistent results, confirming the reliability of digital caliper measurements. These clarifications and additional data have been included in the revised manuscript to enhance the robustness and clarity of our methodology.

H&E images for assisted reading PMID:28285905

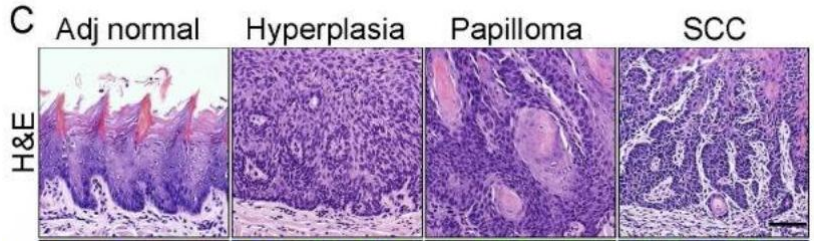

New Figure S1A-C and Supplementary data A and B

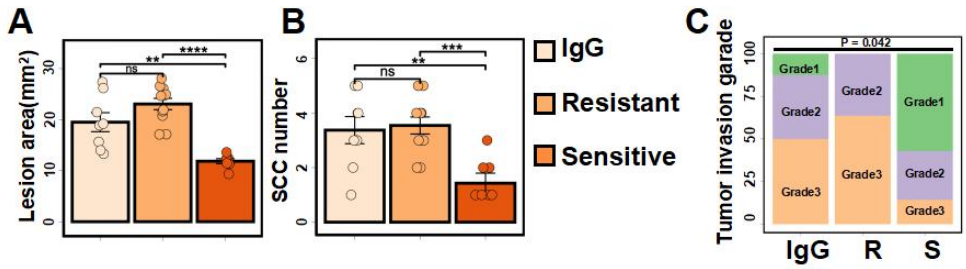

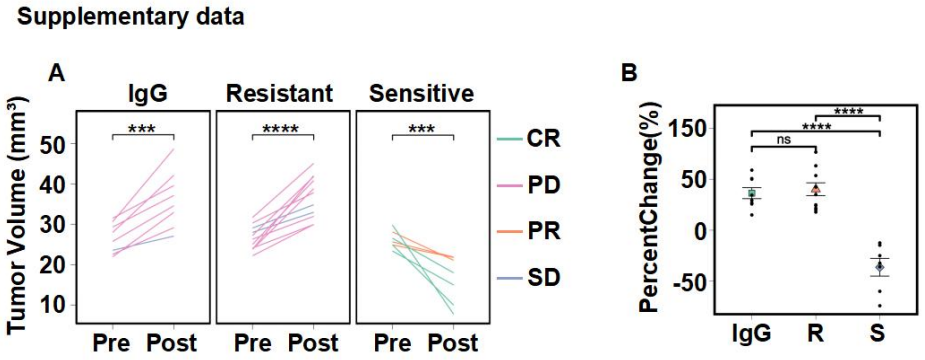

New Figure S5H-J and Supplementary data A and B

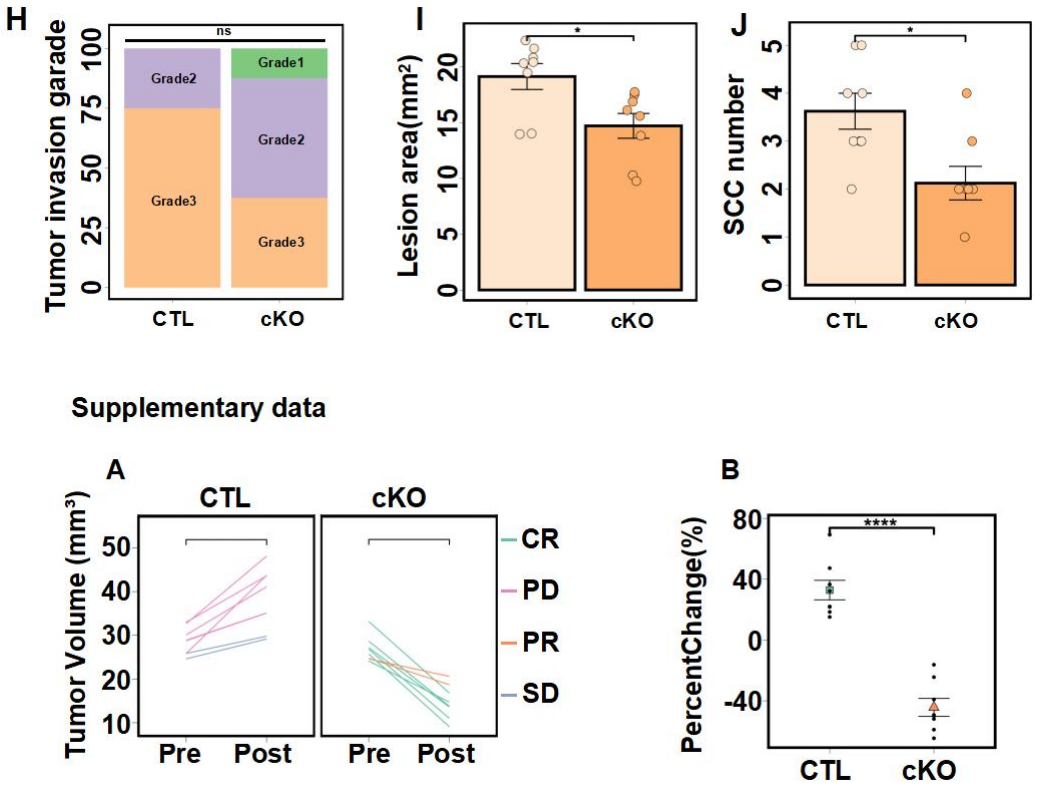

New Figure 3C-E and Supplementary data A and B

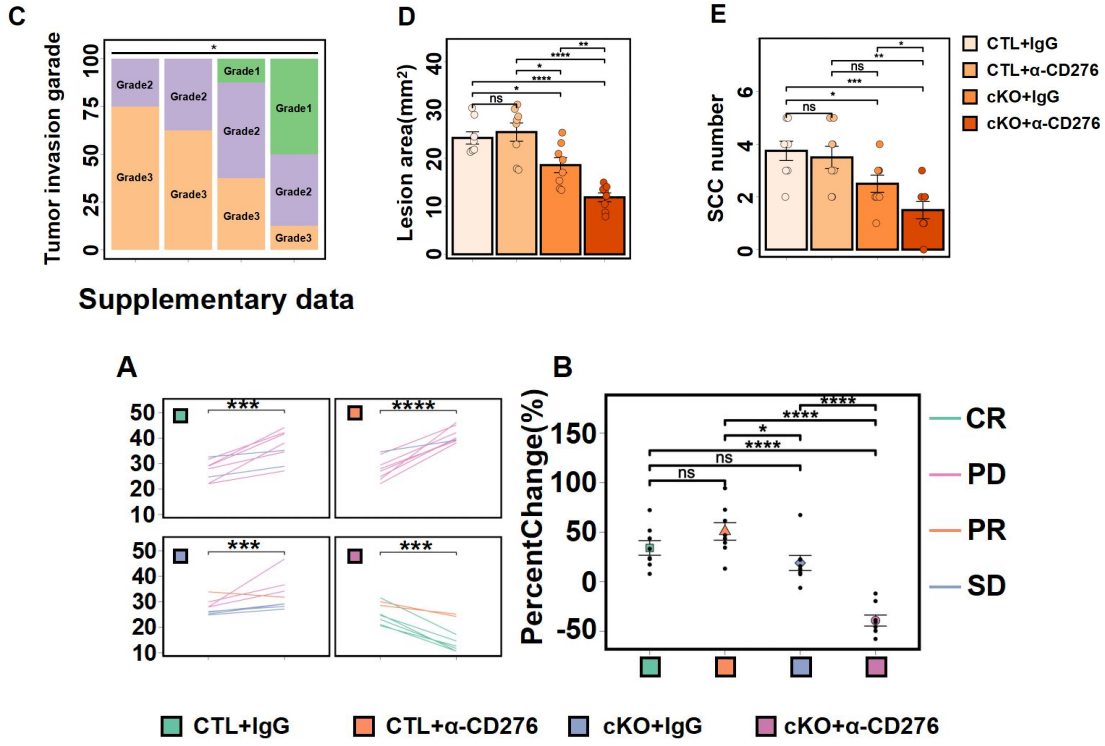

New Figure S1A-C and Supplementary data A and B A and B. Quantification of tongue lesion area (D) and SCC number (E) in in different treatment groups. *P* values were calculated by one-way ANOVA with Tukey's multiple comparison test. C.

Quantification of primary tumor incidence in in different treatment groups. *P* value was calculated by Pearson chi-square test. Supplementary data A. Tumor volume changes in different groups pre- and post-treatment. The different clinical responses are indicated by color: CR (Complete Response), PD (Progressive Disease), PR (Partial Response), and SD (Stable Disease).P values were calculated by two-tailed unpaired Student's t-test. B. Percent change in tumor volume across different groups. *P* values were calculated by one-way ANOVA with Tukey's multiple comparison test.

New Figure S5H-J and Supplementary data A and B H. Quantification of primary tumor incidence in in different treatment groups. *P* value was calculated by Pearson chi-square test. I and J. Quantification of tongue lesion area (I) and SCC number (J) in in different treatment groups. *P* values were calculated by two-tailed unpaired Student's t-test. Supplementary data A. Tumor volume changes in different groups pre- and post-treatment. The different clinical responses are indicated by color: CR (Complete Response), PD (Progressive Disease), PR (Partial Response), and SD (Stable Disease). *P* values were calculated by two-tailed unpaired Student's t-test. B. Percent change in tumor volume across different groups. *P* values were calculated by one-way ANOVA with Tukey's multiple comparison test.

New Figure 3C-E and Supplementary data A and B C. Quantification of primary tumor incidence in in different treatment groups. *P* value was calculated by Pearson chi-square test. D and E. Quantification of tongue lesion area (D) and SCC number (E) in in different treatment groups. *P* values were calculated by one-way ANOVA with Tukey's multiple comparison test. Supplementary data A. Tumor volume changes in different groups pre- and post-treatment. The different clinical responses are indicated by color: CR (Complete Response), PD (Progressive Disease), PR (Partial Response), and SD (Stable Disease). *P* values were calculated by two-tailed unpaired Student's t-test. B. Percent change in tumor volume across different groups. *P* values were calculated by one-way ANOVA with Tukey's multiple comparison test.

3. Given the goal of tumor elimination, it is imperative to delineate Caspase-3 staining on tumor cells over stromal cells. This should be assessed. Current image quality does not allow the readers to thoroughly and unequivocally assess it themselves.

Response: Thank you for your valuable comments. In response to your suggestion to delineate Caspase-3 staining on tumor cells over stromal cells, we have replaced all Caspase-3 staining images where tumor and stromal cells could not be distinctly differentiated. Additionally, we have separately quantified the proportion of Caspase-3 positive cells in tumor and stromal compartments to provide a clear assessment. These modifications aim to better illustrate the goal of tumor elimination and ensure readers can thoroughly and u nequivocally evaluate the data.

New Figure S1F and G

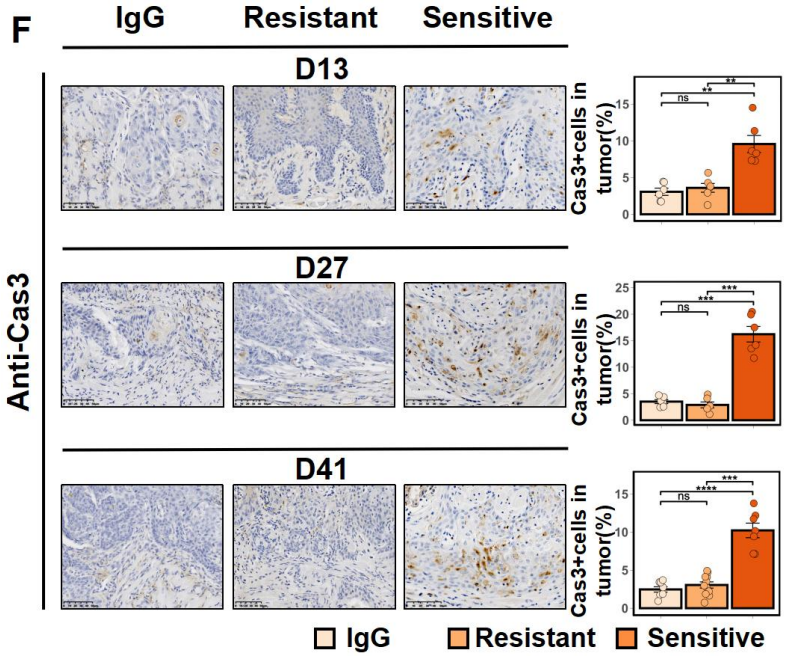

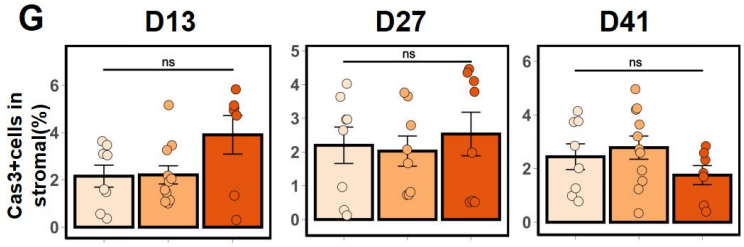

New Figure 6F and G

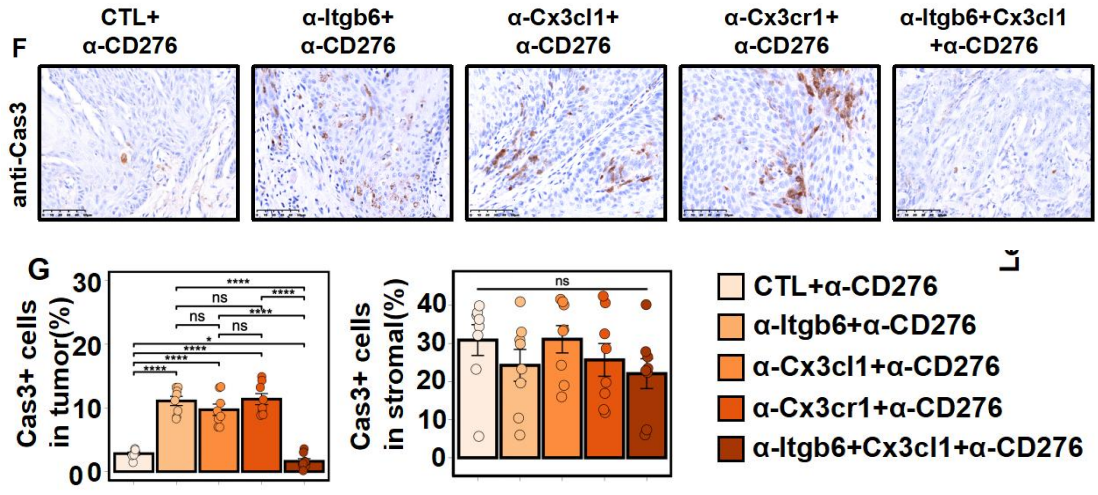

New Figure 8J and K

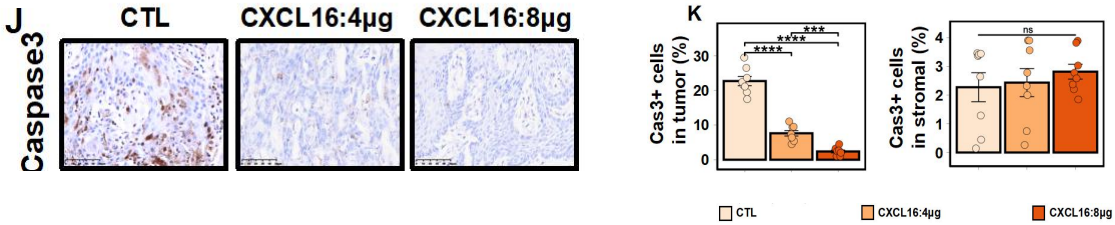

New Figure S1F and G.Representative images of Caspase-3 IHC staining (left) and quantification of percentage of Caspase-3$^+$ cells in tumor cells (right) among different treatment groups and time points. Scale bar, 100μm. Data are presented as mean ± SD (Day 41 IgG=8, Resistant=11, Sensitive=7, Day 13 and 27 n=6). *P* values are presented by one-way ANOVA with Tukey's multiple comparison test. G. Quantification of percentage of Caspase-3$^+$ cells in stromal cells (right) among different treatment groups and time points. Data are presented as mean ± SD (Day 41 IgG=8, Resistant=11, Sensitive=7, Day 13 and 27 n=6). *P* values are presented by one-way ANOVA with Tukey's multiple comparison test.

New Figure 6F and G F F. Representative images of Caspase-3 IHC staining. Scale bar, 100μm. G. Quantification of percentage of Caspase-3$^+$ cells in tumor cells (left) and stromal cells (right) among different treatment groups. Data are presented as mean ± SD (n=8). *P* values are presented by one-way ANOVA with Tukey's multiple comparison test.

New Figure 8J and K J. Representative images of Caspase-3 IHC staining. Scale bar, 100μm. K. Quantification of percentage of Caspase-3$^+$ cells in tumor cells (left) and stromal cells (right) among different treatment groups. Data are presented as mean ± SD (n=8). *P* values are presented by one-way ANOVA with Tukey's multiple comparison test.

REVIEWERS' COMMENTS

Reviewer #2 (Remarks to the Author):

I am satisfied by the response provided by the authors

Reviewer #4 (Remarks to the Author):

This version of the revised manuscript has been improved with very informative experimental design flowcharts. However, some questions remain unanswered, and the data in some figures are difficult to relate to the context.

1. The authors' response to our question, “The mechanism by which PF4+ macrophages regulate CXCR6+CD8+ T cells remains unclear and requires a clearer explanation,” does not seem to be clearly addressed. Are the authors trying to say that “PF4+ macrophages regulate CXCR6+CD8+ T cells via the CXCL-16-CXCR6-CREM axis”?

2. The role of CREM in regulating CXCR6+ CD8+ T cells is unclear. For example, in Figure S12H, it is difficult to draw the conclusion that "sorted PDCD1+ CXCR6+ CD8+ T and GZMB+CXCR6+ CD8+ T cells demonstrated a notable increase in CREM levels within the GZMB+ CXCR6+ CD8+ T cell subgroup." Does this mean that CXCL16 contributes to the low GZMB+/PDCD1+ ratio in CXCR6+ CD8+ T cells? What about the expression of CREM in PDCD1+ CXCR6+ CD8+ T cells when treated with high/low levels of CXCL16?

Reviewer #5 (Remarks to the Author):

The authors have addressed my comments, but it seems some adjustments were not completely fulfilled.

- The detailed explanation on choosing parameters (tumor grade, lesion area, SCC number) is lacking in the manuscript.
- Cas3 staining specific for tumor cells and stromal cells is lacking in figures 2H and 3G.

We sincerely appreciate the invaluable comments and insights provided by the reviewers. We have thoroughly considered their critiques and suggestions, and have made diligent efforts to address all concerns raised. Significant new data have been added to both the main and supplementary figures, directly responding to the issues highlighted in the initial review. As a result, our manuscript has been substantially improved, offering a stronger and clearer presentation of our findings. We are grateful for the reviewers' guidance, which has considerably enhanced our research. Furthermore, we thank the reviewers for their patience during the extended revision process, necessitated by the comprehensive experimental work required. Their understanding and willingness to evaluate the revised manuscript are highly appreciated.

Reviewer #2 (Remarks to the Author):
I am satisfied by the response provided by the authors

Response: We appreciate your positive feedback and are pleased that our responses have satisfactorily addressed your concerns. Thank you for your thorough review and valuable input, which have helped to improve the quality of our manuscript.

Reviewer #4 (Remarks to the Author):
This version of the revised manuscript has been improved with very informative experimental design flowcharts. However, some questions remain unanswered, and the data in some figures are difficult to relate to the context.

Response: Thank you for your constructive feedback and positive response. We appreciate your recognition of the improvements made in the manuscript. To address the remaining questions and clarify the contextual relationship of the data presented in some figures, we will provide detailed responses in the following sections.

1. The authors' response to our question, “The mechanism by which PF4+ macrophages regulate CXCR6+CD8+ T cells remains unclear and requires a clearer explanation,” does not seem to be clearly addressed. Are the authors trying to say that “PF4+ macrophages regulate CXCR6+CD8+ T cells via the CXCL-16-CXCR6-CREM axis”?

Response: Thank you for your constructive comments and suggestions. We apologize for any confusion caused in our previous response. As you correctly pointed out, we aim to demonstrate that PF4+ macrophages regulate CXCR6+ CD8+ T cells via the CXCL-16-CXCR6-CREM axis. We have now supplemented the manuscript with additional explanations and data to clarify this mechanism.

2. The role of CREM in regulating CXCR6+ CD8+ T cells is unclear. For example, in Figure S12H, it is difficult to draw the conclusion that "sorted PDCD1+ CXCR6+ CD8+ T and GZMB+CXCR6+ CD8+ T cells demonstrated a notable increase in CREM levels within the GZMB+ CXCR6+ CD8+ T cell subgroup." Does this mean that

CXCL16 contributes to the low GZMB+/PDCD1+ ratio in CXCR6+ CD8+ T cells? What about the expression of CREM in PDCD1+ CXCR6+ CD8+ T cells when treated with high/low levels of CXCL16?

Response: Thank you for your valuable suggestions. We appreciate your efforts to clarify the role of CREM in regulating CXCR6+ CD8+ T cells. To address your concerns, we have made the following revisions. We conducted Western blot experiments on sorted GZMB+ CXCR6+ CD8+ T cells and PDCD1+ CXCR6+ CD8+ T cells to investigate the expression levels of CREM. The results showed a significant increase in CREM levels within the PDCD1+ CXCR6+ CD8+ T cell subset, suggesting that CREM may mediate the exhaustion process of CXCR6+ CD8+ T cells (Supplementary Figure. 12H). To further examine whether this change is mediated via the CXCL16-CXCR6 axis, we added 100 ng/ml and 800 ng/ml of recombinant CXCL16 protein to the cultures of sorted CD8+ T cells. The results indicated that as the concentration of CXCL16 increased, the expression levels of CREM were significantly upregulated in GZMB+ CXCR6+ CD8+ T cells. Additionally, in the absence of CXCL16, CREM was already highly expressed in PDCD1+ CXCR6+ CD8+ T cells, and its expression further increased with higher concentrations of CXCL16 (Supplementary Figure. 12I).

Supplementary Figure. 12H and I

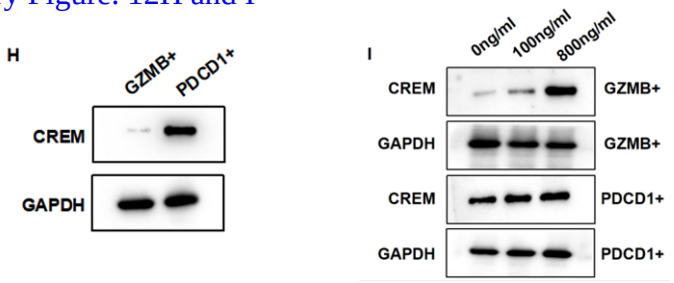

Supplementary Figure. 12. H.Western blotting analysis of CREM in different subsets of CXCR6+CD8+T cells. I.Western blot analysis of CREM in different subsets of CXCR6+ CD8+ T cells under various CXCL16 stimulation conditions.

Reviewer #5 (Remarks to the Author):
The authors have addressed my comments, but it seems some adjustments were not completely fulfilled.
- The detailed explanation on choosing parameters (tumor grade, lesion area, SCC number) is lacking in the manuscript.

Response: Thank you for your insightful suggestions. We have now included detailed explanations and relevant references in the manuscript regarding the parameters used, such as tumor grade, lesion area, and SCC number.

- Cas3 staining specific for tumor cells and stromal cells is lacking in figures 2H and 3G.

Response: Thank you for your suggestion. We have now supplemented the manuscript with specific Caspase-3 staining images for both tumor cells and stromal cells in Figures 2H and 3G.

Figures 2H and I

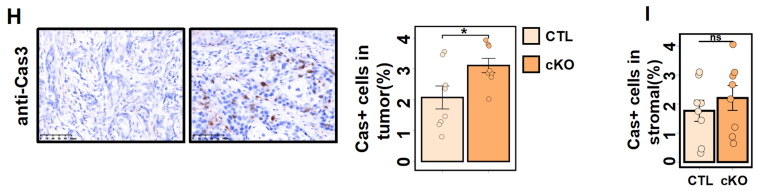

Figures 3G and H